12/2 30 12-22-86 JT 1 of 3 stack all up

DR#0066-3

I-29003

SANDIA REPORT

SAND86—2110 • Unlimited Release • UC—13
Printed November 1986

Release Equation of State of Dry and Water-Saturated Porous Calcite

D. E. Grady, R. L. Moody, D. S. Drumheller

Prepared by
Sandia National Laboratories
Albuquerque, New Mexico 87185 and Livermore, California 94550
for the United States Department of Energy
under Contract DE-AC04-76DP00789

Issued by Sandia National Laboratories, operated for the United States Department of Energy by Sandia Corporation.

Printed in the United States of America
Available from
National Technical Information Service
U.S. Department of Commerce
5285 Port Royal Road
Springfield, VA 22161

NTIS price codes
Printed copy: A04
Microfiche copy: A01

SAND--86-2110

DE87 003589

Distribution
Category UC-13

SAND86-2110
Unlimited Release
Printed November 1986

Release Equation of State of Dry and Water-Saturated Porous Calcite

D. E. Grady, R. L. Moody, and D. S. Drumheller
Solid Dynamics Department
Sandia National Laboratories

ABSTRACT

Equation of state data on calcite obtained from shock compression and release wave experiments are reported. Powder gun and two-stage gun impact technology, along with time-resolved velocity interferometry, are used to produce and measure planar shock and release wave states. Experiments are performed on crystalline calcite and on dry- and water-saturated porous calcite at shock pressures ranging from 10 to 66 GPa. Developmental work required to perform high-pressure shock-wave experiments on porous samples with the two-stage gas gun is described. Lagrangian analysis methods are used to determine pressure-density release paths from measured wave profiles. A high-pressure phase change in calcite has been identified from the release-wave data. Calculational results obtained using a model based on a theory of immiscible mixture are compared with the experimental data.

Contents

1 INTRODUCTION 3

2 BACKGROUND 4

3 SUMMARY 5

4 EXPERIMENTAL EQUATION-OF-STATE OF CALCITE 7
- 4.1 Release-Wave Measurements on Crystalline Calcite . . . 7
  - 4.1.1 Experimental Method . . . 7
  - 4.1.2 Experimental Results . . . 7
  - 4.1.3 Experimental Analysis . . . 10
  - 4.1.4 Discussion of the Release-Wave Data . . . 14
- 4.2 Release-Wave Measurements on Dry-Porous and Water-Saturated Calcite . . . 14
  - 4.2.1 Calcium Carbonate Powder . . . 14
  - 4.2.2 The Compaction Process . . . 17
  - 4.2.3 Two-Stage Gun Target Configuration . . . 17
  - 4.2.4 Two-Stage Gun Projectile . . . 17
  - 4.2.5 Preliminary Experiments on Dry Porous Calcite . . . 17
  - 4.2.6 Double Shock Experiments . . . 20
  - 4.2.7 Experimental Methods on Water-Saturated Calcite . . . 20
  - 4.2.8 Experiments on Dry and Water-Saturated Porous Calcite . . . 22
- 4.3 Analysis of Dry and Water-Saturated Porous Calcite Experiments . . . 22
- 4.4 Pressure-Density Release Paths for Dry and Water-Saturated Porous Calcite . . . 26

5 EQUATION-OF-STATE MODELING OF POROUS CALCITE 35
- 5.1 Background . . . 35
- 5.2 Theory . . . 36
- 5.3 Comparison of the Theory with Hugoniot Data . . . 39
- 5.4 Comparison of the Theory with Experiments CA-16 thru 21 on Dry and Water-Saturated Porous Calcite. . . . 41

6 CONCLUSIONS AND RECOMMENDATIONS FOR FURTHER STUDY 57

7 REFERENCES 59

1 INTRODUCTION

A combined exploratory and calculational program was initiated by the Defense Nuclear Agency (DNA) to better understand the cratering dynamics responsible for the Pacific Eniwetok Atoll nuclear craters. The Pacific Eniwetok Atoll Cratering Exploration (PEACE) program is focused on evaluation of geological conditions in the immediate vicinity of the Pacific craters. The Pacific Proving Ground (PPG) calculational program will analyze specific cratering events to both support the PEACE program and test theoretical mechanisms proposed for the cratering process.

In support of the PPG calculational effort, a program to obtain material property data necessary to successfully calculate cratering in the carbonate rock and minerals constituting the PPG atolls was also initiated. In support of this effort, Sandia National Laboratories has undertaken studies to investigate the unloading response of carbonate minerals (and water-mineral mixtures) from high-pressure Hugoniot states between about 10-100 GPa. The present document reports on the progress of that work.

2 BACKGROUND

When the effort to measure high-pressure Hugoniot unloading states was initiated in early 1984, a program was identified, which was consistent with the needs of DNA and the particular expertise of the SNLA Solid Dynamics Department. It was decided to focus initially on the behavior of pure calcium carbonate in the solid, dry-porous, and wet-porous state. The solid material was theoretically dense z-cut crystalline calcite. Porous samples (near 50% porosities) were prefabricated from calcite powder.

This particular experimental approach was necessary for several reasons. The small samples needed in two-stage gas-gun experiments, using time-resolved velocity interferometry diagnostics, require the use of fine-grain, homogeneous samples for optimum accuracy. Previous shock-wave work on calcite rocks and minerals indicate that microstructural differences in the initial state become unimportant at shock pressures in excess of 10 GPa. Consequently, unloading behavior should be controlled predominantly by the thermodynamic character of the mineral constituents.

With a two-stage gun facility, unloading states in solid material from Hugoniot pressures between about 10-100 GPa can be achieved. Distended samples with initial porosities near 50% limit the peak pressures achievable in a single-shock experiment. Double-shock experiments were performed, therefore, in which unloading from significantly higher shock pressures could be achieved.

Crystalline calcite samples and measurement techniques were immediately available and, consequently, this portion of the study was completed early in the program. Testing on dry-porous and water-saturated samples required a significant amount of technique development, and a substantial part of the later effort was focused on these problems.

3 SUMMARY

The work undertaken in the present study falls into three general categories. First was the development of techniques for performing shock-wave equation-of-state experiments on dry-porous and water-saturated geological materials using a two-stage light gas gun facility and laser interferometry diagnostics. Second was the performance of shock-wave equation-of-state experiments on crystalline, dry-porous, and water-saturated calcite. And third was the development and application of an immiscible mixture theory for describing the thermodynamic response during shock-wave loading of a calcite-water-void mixture.

Early in the study, a series of impact shock-wave experiments were conducted on z-cut crystalline calcite. A single-stage powder gun was used to perform these tests and six successful experiments to shock pressures between about 10–30 GPa were completed. The experiments were designed to measure continuous shock-loading and release-wave profiles. The most significant result of this effort was the identification, for the first time, through the observation of a rarefaction shock wave on release, of a high-pressure phase transformation in calcite. The transformation occurs between 12-14 GPa on pressure release, accompanied by a volume strain of 3–5%.

Substantial effort during this study focused on developing techniques for performing high-pressure shock-wave experiments on dry-porous and water-saturated materials. Samples were constructed through compaction of calcite powders. Methods were developed to produce uniform and controlled porous samples (porosities obtained were near 50%). Techniques were determined for water saturating porous samples. Procedures were found for performing shock experiments on porous and water-saturated samples within the near-vacuum environment required in two-stage gas gun testing. Finally, methods were determined for obtaining laser-interferometry velocity profiles at the high temperature, granulated interface between the calcite sample and a laser window material.

Two different methods were used to obtain shock-wave equation-of-state data on dry-porous and water-saturated calcite. In the first, dry-porous samples were impacted with thin aluminum flyers and backed by transparent PMMA (plexiglas) plates. Interface motion between the sample and PMMA window was monitored. This method was limited to pressures below about 20 GPa because of loss of transparency in PMMA at pressures in excess of this value (Chhabildas and Asay, 1979). Two successful experiments were completed using this approach. In the second method, lithium fluoride was used as a laser window material. Transparency in lithium fluoride is known to be retained to shock pressures of at least 180 GPa (Wise and Chhabildas, 1985). Because lithium fluoride has a shock impedance significantly higher than the dry-porous and water-saturated calcite samples, pressure is achieved through a double-shock process. This feature was utilized in the equation-of-state experiments and release data from pressures as high as 66 GPa were obtained. A total of six experiments on dry-porous and water-saturated calcite were successfully completed. In all experiments, complete loading and release-wave profiles were measured. In the final set of experiments, the design actually provided for a second reshock and release. Considerable care was exercised in sample preparation and interferometry measurement and a high degree of resolution in wave structure was obtained. One difficulty in the tests occurred in measuring time-of-impact which determines absolute transit times and shock velocities. Errors in these values represent a weakness of the data and an area for future improvement.

Finally, a model for describing the response of dry-porous and water-saturated calcite based

on a theory of immiscible mixtures was developed. The theory separately accounts for the equations of state of calcite and water. Void is considered a further constituent. The components are joined in the theory through a mechanical and thermal mixing rule. Compatibility of the model with contemporary wave propagation codes was an important thrust of the development. The model was based on Hugoniot data for dry and water-saturated data from Kalishnikov, *et al.* (1973) and release data from earlier efforts in the current study. The ability of the model to predict the diverse data produced in the present program represented an encouraging aspect of the study.

4 EXPERIMENTAL EQUATION-OF-STATE OF CALCITE

4.1 Release-Wave Measurements on Crystalline Calcite

4.1.1 Experimental Method

Samples of optical grade Icelandic spar crystals of calcite were obtained from Karl Lambrecht Corp., Chicago, Illinois. Samples were cut on planes normal to the crystal Z axis. The direction of shock propagation was along the Z axis.

The experimental configuration is illustrated in Figure 1. Calcite samples are lapped flat and parallel, and mounted in a target ring. A lithium fluoride laser window material with an approximately 2000-Å diffusely-reflecting vapor-deposited aluminum film is epoxy-bonded to the back surface of the calcite sample. The shock-wave motion is measured at the center of this interface with laser velocity interferometry (VISAR) techniques (Barker and Hollenbach, 1972).

Metal discs are mounted on a projectile body. A void cavity is maintained immediately behind the disc to provide an unloading wave following shock loading. The projectiles are accelerated in an 88-mm diameter powder gun facility capable of achieving a maximum velocity of approximately 2.2 km/s. Shock loading is achieved by planar impact of the metal disc on the calcite sample. Electrical shorting pins are used to measure impact velocity and planarity, and to establish timing for oscilloscope and digitizer recording of the VISAR signal.

In several cases, experiments at the same impact velocity, but with different calcite sample thicknesses, were performed. This allowed incremental determination of the wave velocity and calculations of the continuous stress-volume response through integrations of the appropriate Riemann invariant. These experiments also provided a test of centered-wave behavior which was assumed at the shock amplitudes where only one profile was measured.

4.1.2 Experimental Results

Aluminum impactors were used in the experiments to generate shock pressures of 11.5 and 17.0 GPa, which provided for a nearly complete release from the shock state. Stainless steel was used for the highest shock pressure experiments (26.5 GPa) and only partial unloading was achieved.

The impact experiments on theoretical density ($\rho_o = 2710\ kg/m^3$) crystalline calcite are summarized in Table 1. Hugoniot states measured in these experiments are shown in Figure 2 and compared with other Hugoniot data on various calcium carbonate rocks and minerals. The numbers in parentheses indicate the number of tests performed at each stress level. As noted by Ahrens and Gregson (1964), Hugoniot data above about 10 GPa are not dependent on whether single crystal mineral or polycrystalline rock samples are used as starting material. Consequently, the shock and unloading states measured in these experiments should provide a good crystalline density baseline against which the dry porous and water-saturated data can be compared.

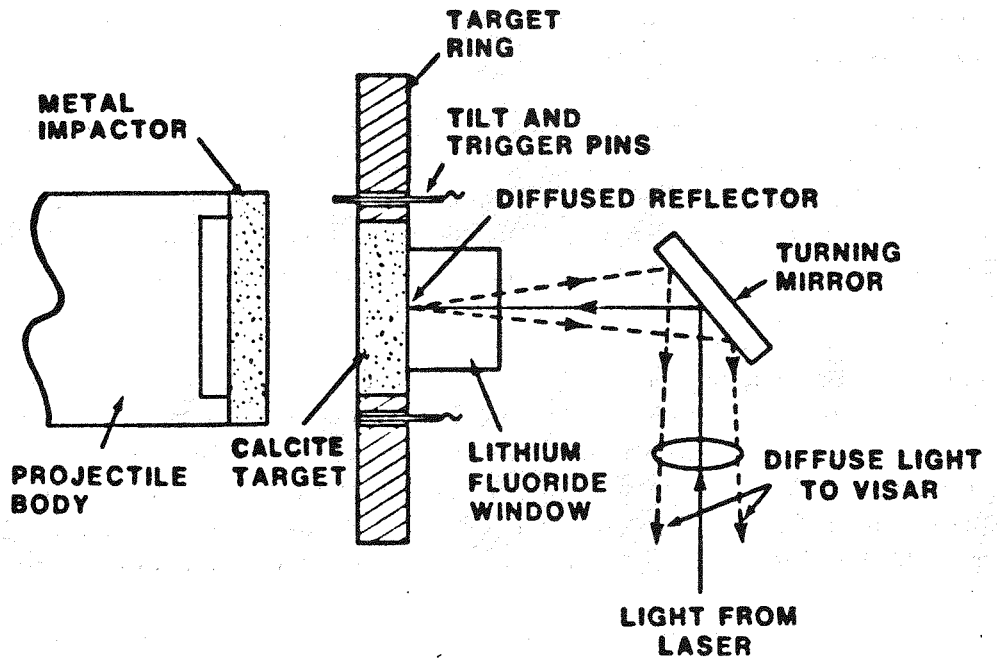

Figure 1: Impact configuration for crystalline calcite shock and release wave experiments.

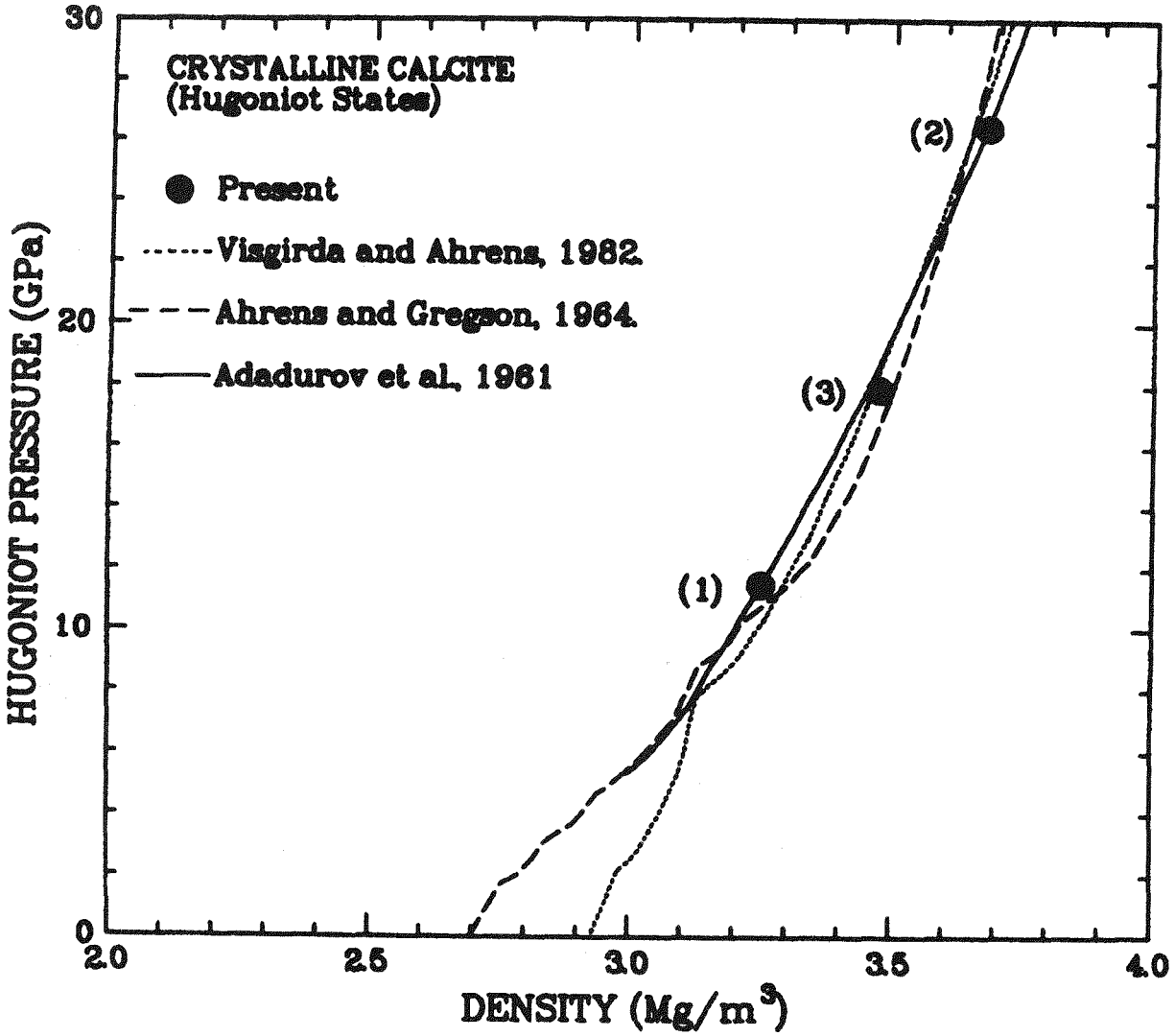

Figure 2: Hugoniot states for shock-compressed calcite. The numbers in parentheses represent the number of experiments at each Hugoniot pressure level.

TABLE 1
Crystalline Calcite Data

Exp. No.	Sample Thickness (mm)	Impactor Thickness (mm)	Impactor Material	Impact Velocity (km/s)	Window Material	First Arrival Velocity (km/s)	Maximum Pressure (GPa)	Maximum Strain
CA-1	5.054	2.645	aluminum	2.170	LiF	5.75*	17.9	0.223
CA-2	3.020	2.634	aluminum	2.152	LiF	5.75*	17.9	0.223
CA-3	8.035	2.582	aluminum	2.171	LiF	5.75*	17.9	0.223
CA-4	6.101	2.116	stainless steel	2.172	LiF	6.05*	26.4	0.266
CA-5	2.071	2.106	stainless steel	2.154	LiF	6.05*	26.4	0.266
CA-8	5.079	2.601	aluminum	1.521	LiF	5.75*	11.5	0.167

*Calculated from previous data on Z-cut calcite (Grady, 1983).

The first series of experiments performed were CA1, CA2, and CA3. Wave profiles measured in these tests are shown in Figure 3. Sample thicknesses were approximately 2, 5, and 8 mm (see Table 1). A Hugoniot pressure of 17.9 GPa was achieved through two loading waves. The 1.5 GPa precursor is due to the calcite I-II-III transformation and yielding. Unloading occurs through regions of isentropic release separated by a nearly discontinuous drop of about 6 GPa through a rarefaction shock wave.

To achieve higher stress levels with the powder gun facility, higher impedance stainless steel impactors were used at near maximum velocity. The wave profiles obtained from these experiments (CA4, CA5) are provided in Figure 4. At this amplitude, the precursor was overdriven and loading to the Hugoniot pressure of 26.4 GPa occurred through a single shock wave. On release, the stainless steel impedance is higher than calcite and unloading occurs through two wave reverberations in the stainless steel impactor. The rarefaction shock is observed just prior to the plateau preceeding the second reflection.

Two further experiments with tungsten impactors were attempted to obtain higher Hugoniot pressures; however, the tungsten discs failed during the acceleration phase on the powder gun due to the void behind the discs.

The final high pressure experiment (CA8) achieved a Hugoniot pressure of 11.5 GPa. The profile is shown in Figure 5. No rarefaction shock was observed in the smoothly dispersive release wave from this test.

4.1.3 Experimental Analysis

Continuous loading and release stress-strain data were determined at each Hugoniot pressure level by incrementally determining wave velocities and integrating the appropriate Riemann invariants. Within this process, corrections for impedance differences between the lithium fluoride window and sample material are also made. The details of this method are described

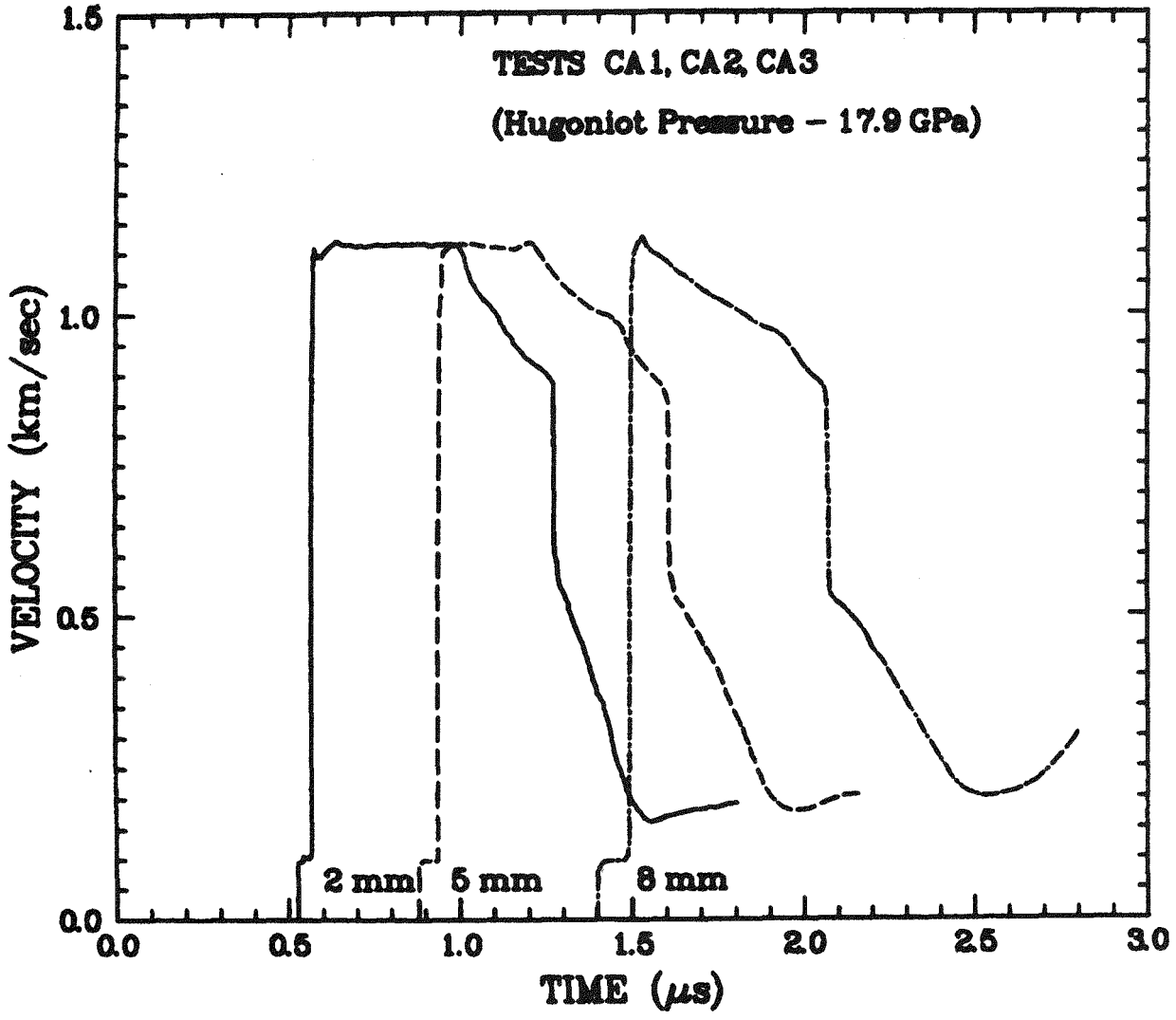

Figure 3: Wave profiles for 17.9 GPa shock compression experiments on crystalline calcite.

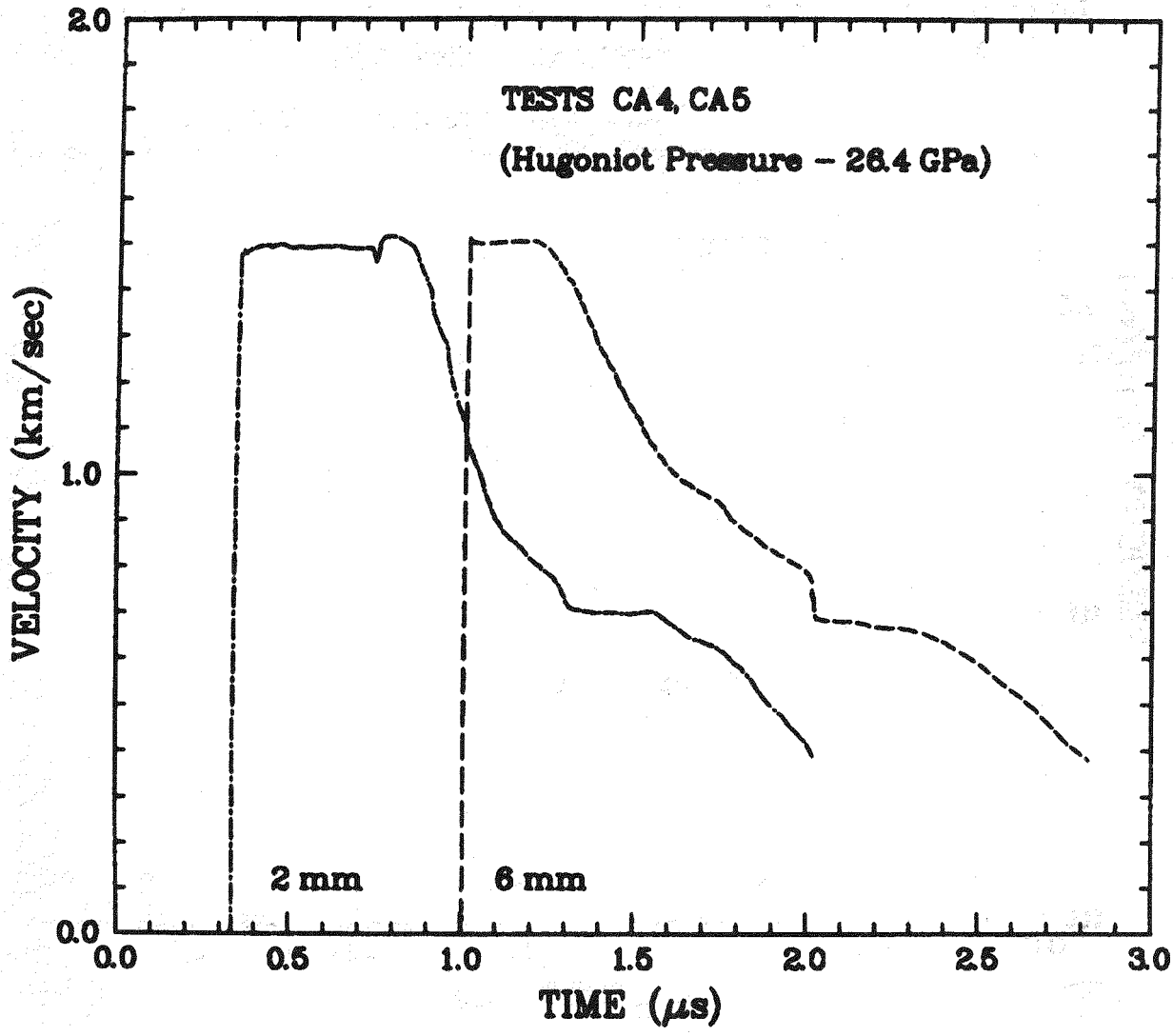

Figure 4: Wave profiles for 26.5 GPa shock compression experiments on crystalline calcite.

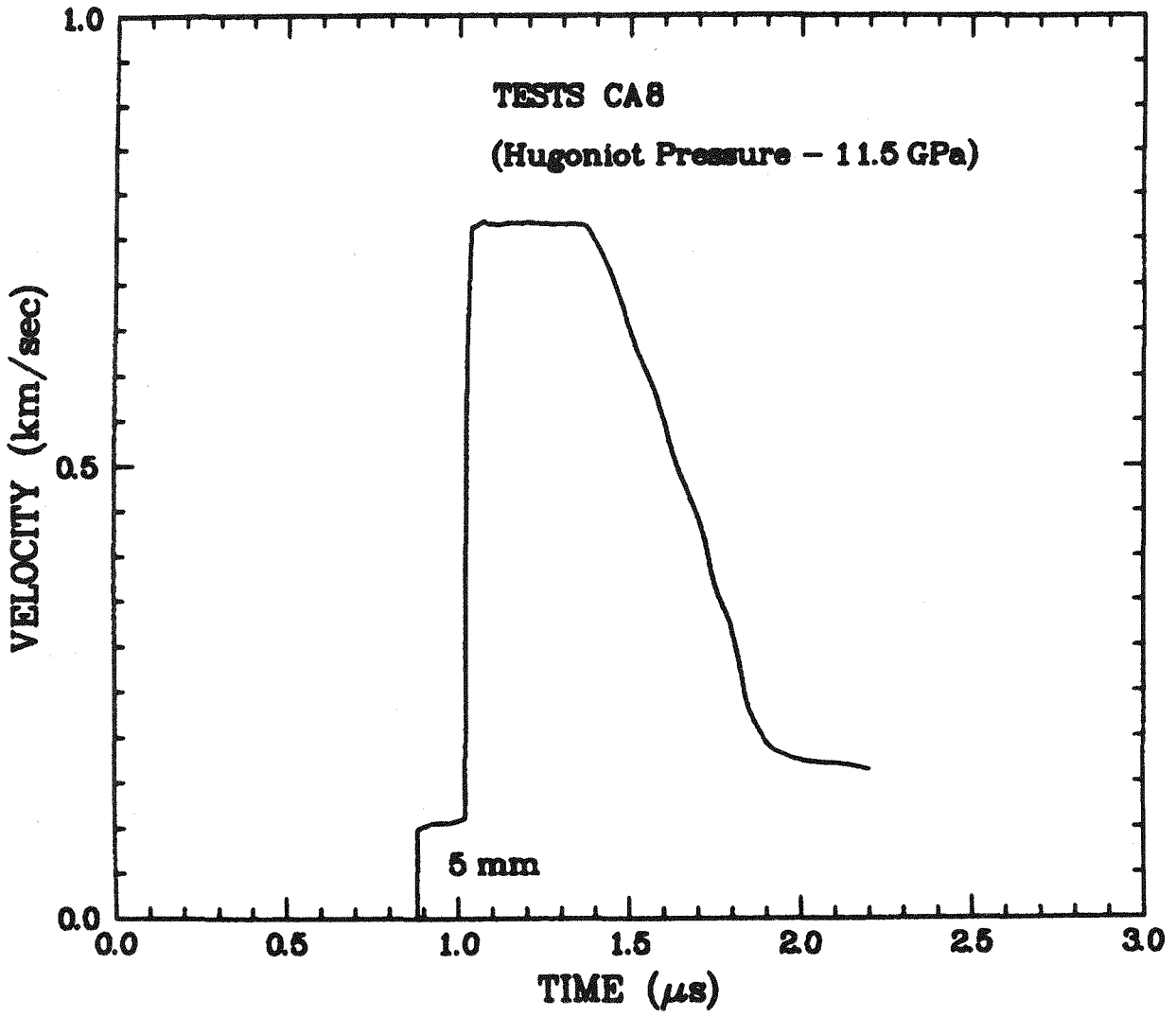

Figure 5: Wave profile for the 11.5 GPa shock compression experiments on crystalline calcite.

by Grady and Young (1976). The stress-strain data obtained from this reduction process are provided in Figure 6.

4.1.4 Discussion of the Release-Wave Data

Unloading paths for the present shock-wave data between 20-30 GPa are compared with other Hugoniot data for calcite (Adadurov, *et al.*, 1961; Ahrens and Gregson, 1964) and aragonite (Visgirda and Ahrens, 1982) in Figure 7. The release paths within this pressure range appear to lie near the Hugoniot. The significant complication is the occurrence of a high pressure phase transition in the calcium carbonate mineral near 12-14 GPa, with a transformation volume strain between 3–5%. No indication of this phase change is provided by the structure of the deformational loading wave. This is a consequence of the low-pressure calcite I-II-III transition which has the effect of starting with a slightly distended material and causes the deformation shock path (Rayleigh line) to miss the transition inflection point on loading.

The most important shock-wave feature of the phase transition occurs during unloading in terms of a nearly discontinuous rarefaction shock causing an abrupt stress drop of approximately 6 GPa. The high-pressure calcite phase may be equivalent to the high-pressure state of aragonite or a further metastable phase of calcite.

The lower portions of the three release paths (near $\rho \simeq 3000\ kg/m^3$) indicate a significant thermal pressure component. The magnitude corresponds to a Grüneisen parameter of $\gamma \simeq 1.5$, which is close to the value measured by other methods.

4.2 Release-Wave Measurements on Dry-Porous and Water-Saturated Calcite

A significant portion of the experimental work focused on development of techniques for performing high-pressure unloading wave experiments in porous calcium carbonate. Previous studies of this type have used porous rock or commercial chalk samples. Our investigations have indicated that such samples are not sufficiently homogeneous for accurate velocity interferometry and would not allow adequate variability in porosity for the thermodynamic studies of interest.

Consequently, we have chosen to construct porous compacts from calcium carbonate powders and perform Hugoniot shock- and release-wave experiments through two-stage gun impact up to approximately 5.5 km/s. Similar tests should be performed on reconstituted PPG material but have not been performed. There is little previous work to guide such efforts; thus, the work reported here has been developmental in nature.

4.2.1 Calcium Carbonate Powder

We have obtained commercially available powders of pure calcium carbonate in the calcite I phase from Atlantic Equipment Engineers (New Jersey). The powder requested was pre-sieved to 30-μm maximum particle size. Optical microscopy of powder samples indicate most particles are closer to several μm in diameter and larger particles are aglomerates of the smaller particles. Due to electrostatic attraction and aglomeration effects, it is difficult to sieve calcium carbonate below 30 μm.

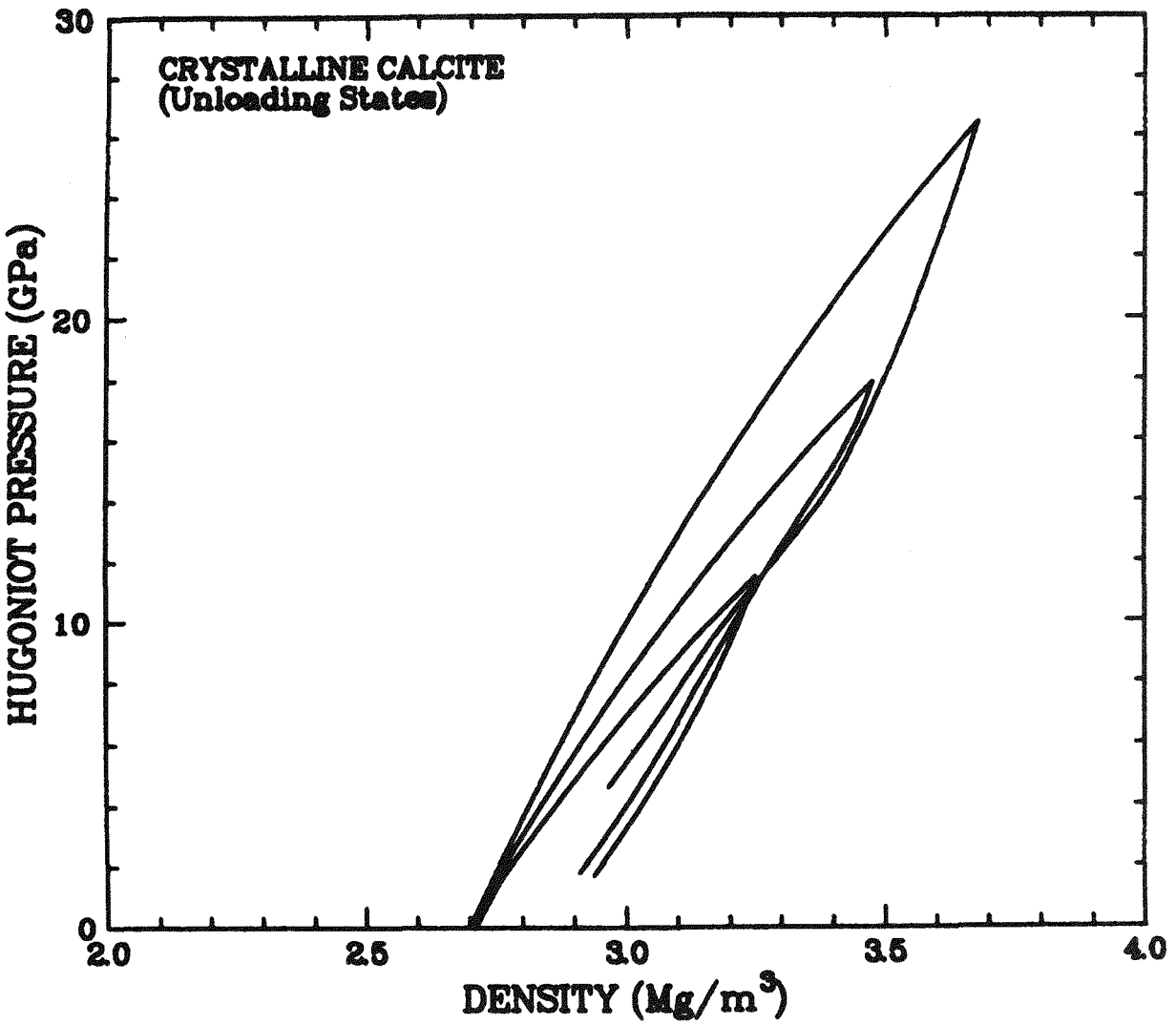

Figure 6: Compression and unloading paths for shock compressed crystalline calcite.

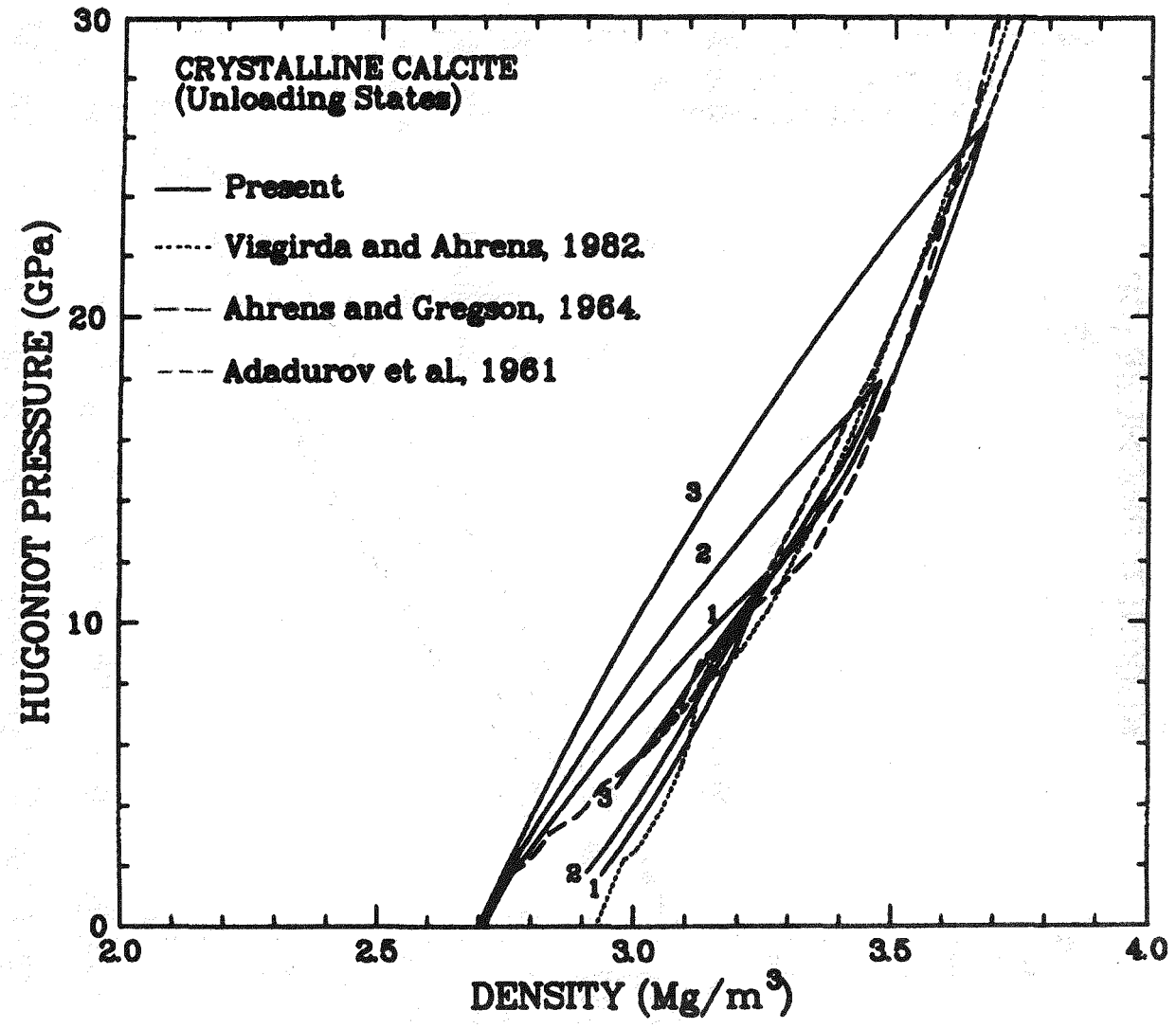

Figure 7: Comparison of unloading curves with Hugoniot data for crystalline calcite.

4.2.2 The Compaction Process

Preparation of porous calcite samples was performed using standard powder compaction methods. Specimens in the form of discs approximately 20 mm in diameter and 2 mm in thickness, with porosities between 15 and 40% were desired. A steel cylindrical die and punch were constructed. Compacts were prepared by placing a fixed mass of powder within the die and hydraulic pressing with the punch until a sample volume commensurate with the required porosities was achieved. Specimens prepared by this method with porosities between 15 and 40% were competent and visually homogeneous.

It was found that the calcite specimens prepared by this compaction process have insufficient intrinsic strength to survive the usual two-stage gun target preparation routine. To solve this problem the compaction process was performed in the actual target fixture to be used in the impact experiment.

4.2.3 Two-Stage Gun Target Configuration

The target assembly designed for the first release-wave experiments in porous calcite is illustrated in Figure 8. The projectile impacts the thin aluminum front plate which is at the bottom of the assembly shown in the Figure. The calcite powder is compacted to the desired porosity with the laser window. The window is then rigidly fixed to the assembly. Thus, the porous sample is immediately contained within the target fixture and specimen strength is not an issue.

4.2.4 Two-Stage Gun Projectile

Until recently, it was not considered feasible to mount an impactor plate on a two-stage gun sabot having a void behind the central region of the plate. The method illustrated in Figure 9 has been successfully used by Asay, *et al.* (1985). The impactor and supporting plate are fabricated of a high-strength aluminum alloy. Dimensions of the plates and cavity are designed to withstand the high acceleration forces experienced in achieving 6 km/s impact velocity. This projectile was used on the porous calcite experiments to achieve both shock loading and release states in the sample.

4.2.5 Preliminary Experiments on Dry Porous Calcite

A preliminary series of impact experiments using the two-stage gun facility was initially performed to test the developmental concepts. In these experiments, dry porous samples (approximately 40% void volume) were shock-loaded to Hugoniot pressures between about 15 to 20 GPa and then released. PMMA (polymethylmethacrelate) was used as the laser window material. It was discovered that laser-light reflectivity was immediately lost upon arrival of the shock-wave at the sample-window interface, presumably due to intense shock heating or granularity of the sample material. It was found necessary to insert a thin ($\sim$ 0.1 mm) mylar shim between the sample and window to maintain integrity of the reflecting interface during transmission of the loading and release wave.

Two experiments were successfully completed. The shock and release profiles are provided in Figure 10. Impact data are provided in Table 2.

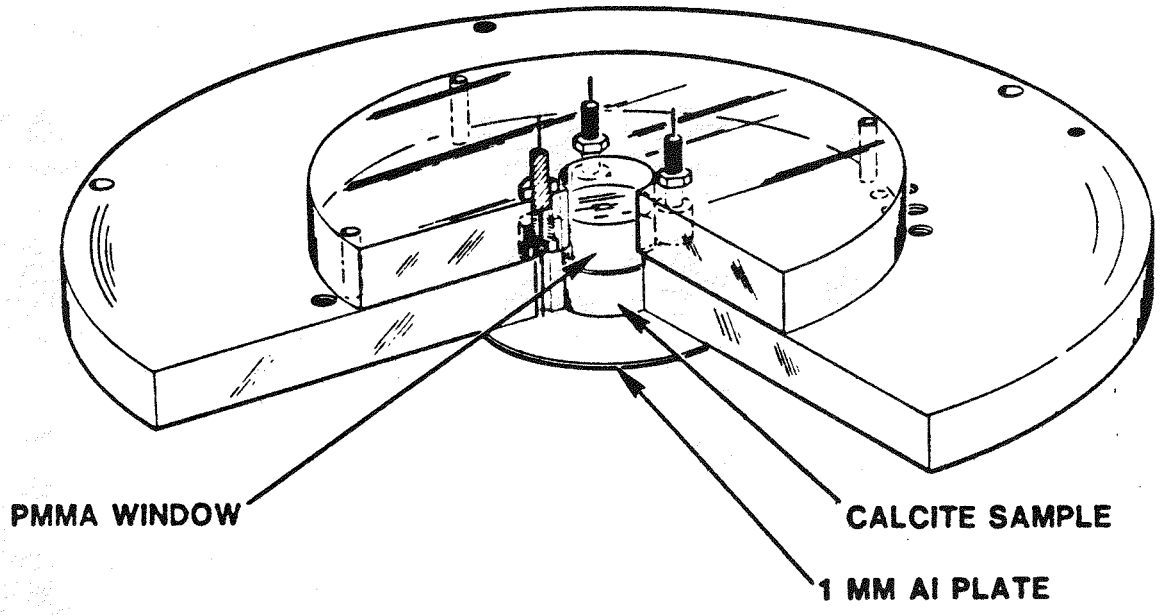

Figure 8: Target configuration for shock compression and release experiments on porous calcite.

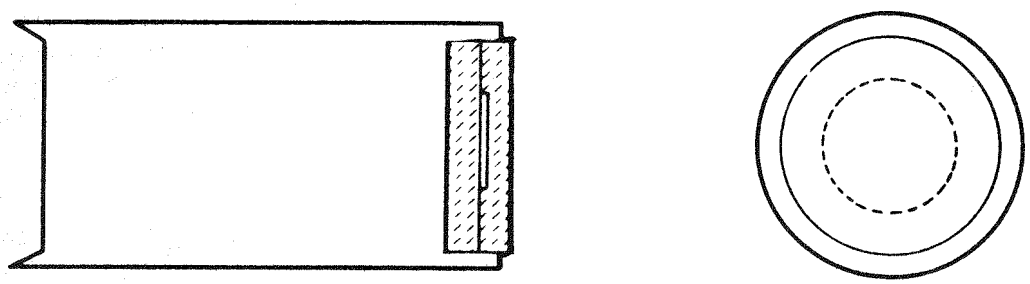

Figure 9: Projectile for two-stage gas gun impact experiments on porous calcite.

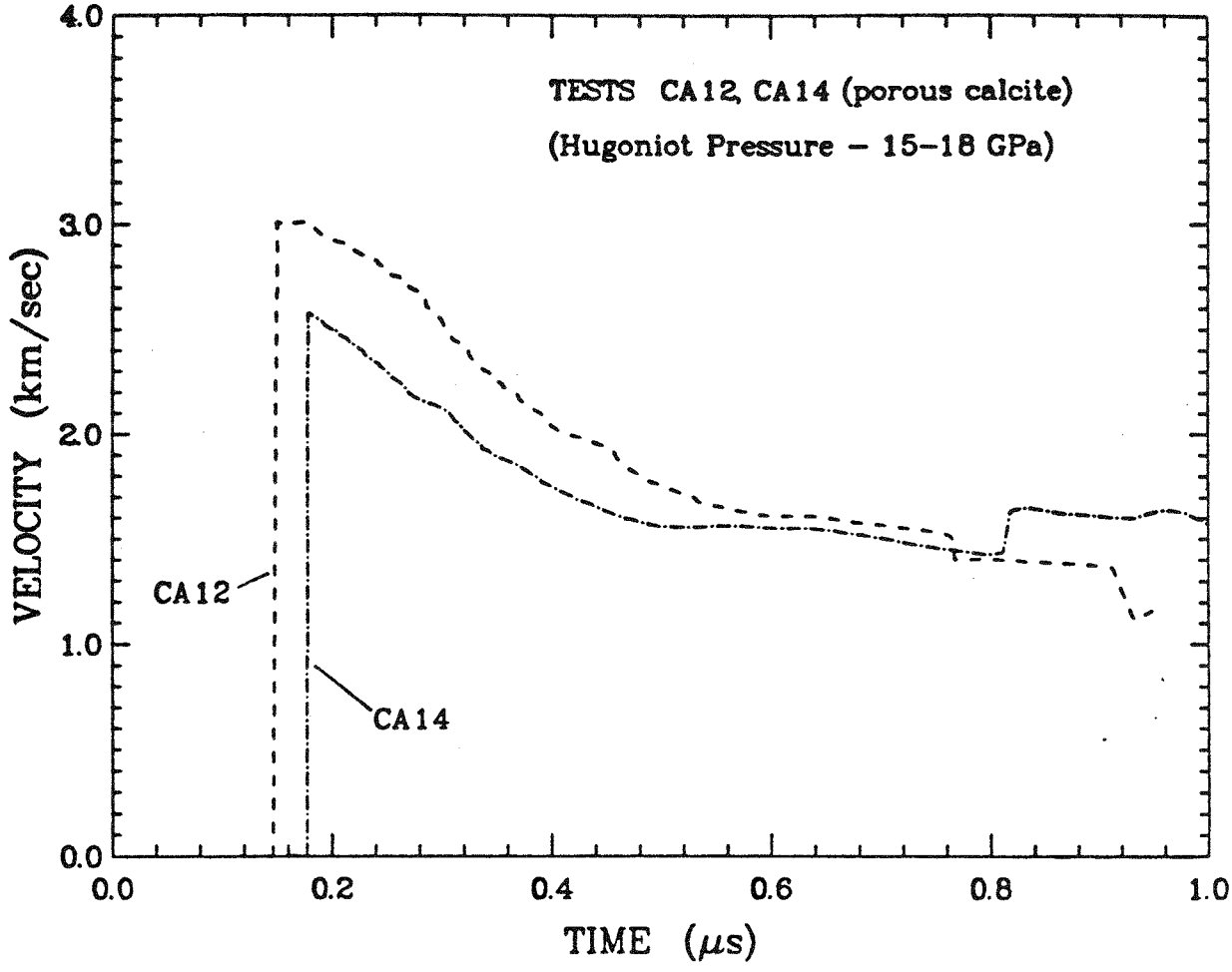

Figure 10: Wave profile measurements on approximately 40% dry porous calcite.

TABLE 2
Dry Porous Calcite Data

Exp. No.	Impactor Thickness (mm)	Impact Buffer Thickness (mm)	Sample Thickness (mm)	Sample Density (kg/m^3)	Window Material	Window Buffer Thickness (mm)	Impact Velocity (km/s)	Shock* Velocity (km/s)
CA-12	1.503	0.962	2.265	1600	PMMA	0.121	3.47	4.84
CA-13	1.491	1.034	2.395	1603	PMMA	0.107	3.03	4.40

*Not measured. Estimated from the data of Kalisnikov, *et al*, 1983.

Release paths for the experiments CA-12 and CA-13 calculated from the measured wave profiles are shown in Figure 11 and compared with the Hugoniot and release paths for crystalline calcite.

4.2.6 Double Shock Experiments

Although the PMMA window material provides a reasonably close impedance match for the Hugoniot response of the porous calcite, it is limited in use to shock pressures below approximately 20 GPa due to a loss of transparency at pressure above this level (Chhabildas and Asay, 1979). Lithium fluoride (LiF) is currently the only laser window material which remains transparent at pressures significantly higher than this value (Wise and Chhabildas, 1985). Its properties provide a poor impedance match for the Hugoniot behavior of the porous calcite, but provide a reasonably good impedance match for the unloading response of the compressed calcite.

Since the LiF is significantly higher in impedance than the porous calcite, the effect is to subject the calcite sample to a reflected second shock which approximately doubles the shock pressure in the sample. Thus the target assemblies were designed such that unloading from the projectile impact relieved the calcite from the double shock state. Peak pressures in the shock compressed calcite in excess of 65 GPa were achieved by this method.

4.2.7 Experimental Methods on Water-Saturated Calcite

Considerable effort was required in finding a technique for preparing satisfactory samples of water-saturated porous calcite. First, it was difficult to water-saturate the 30-μm calcite powder used in the preliminary porous calcite study. A calcite powder was sieved and the powder passing a 125-μm sieve but retained on a 63-μm sieve was accepted as the sample material. It compacted well and was readily water-saturated. A prescribed mass of calcite powder was compacted to a desired porosity by the methods described earlier and then water was introduced with a syringe until saturation was achieved. The sample was then recompacted until water appeared around the punch. It was found that the LiF window could not support the compacting pressure and, therefore, another punch was used initially to achieve the desired volume and then replaced by the LiF window after which only a modest pressure was applied to insure saturation. It was observed that a small amount of swelling occurred when the water was introduced which could not be completely removed. Since the volume and mass of calcite were known, the fractions of each component could be calculated readily. The window was then

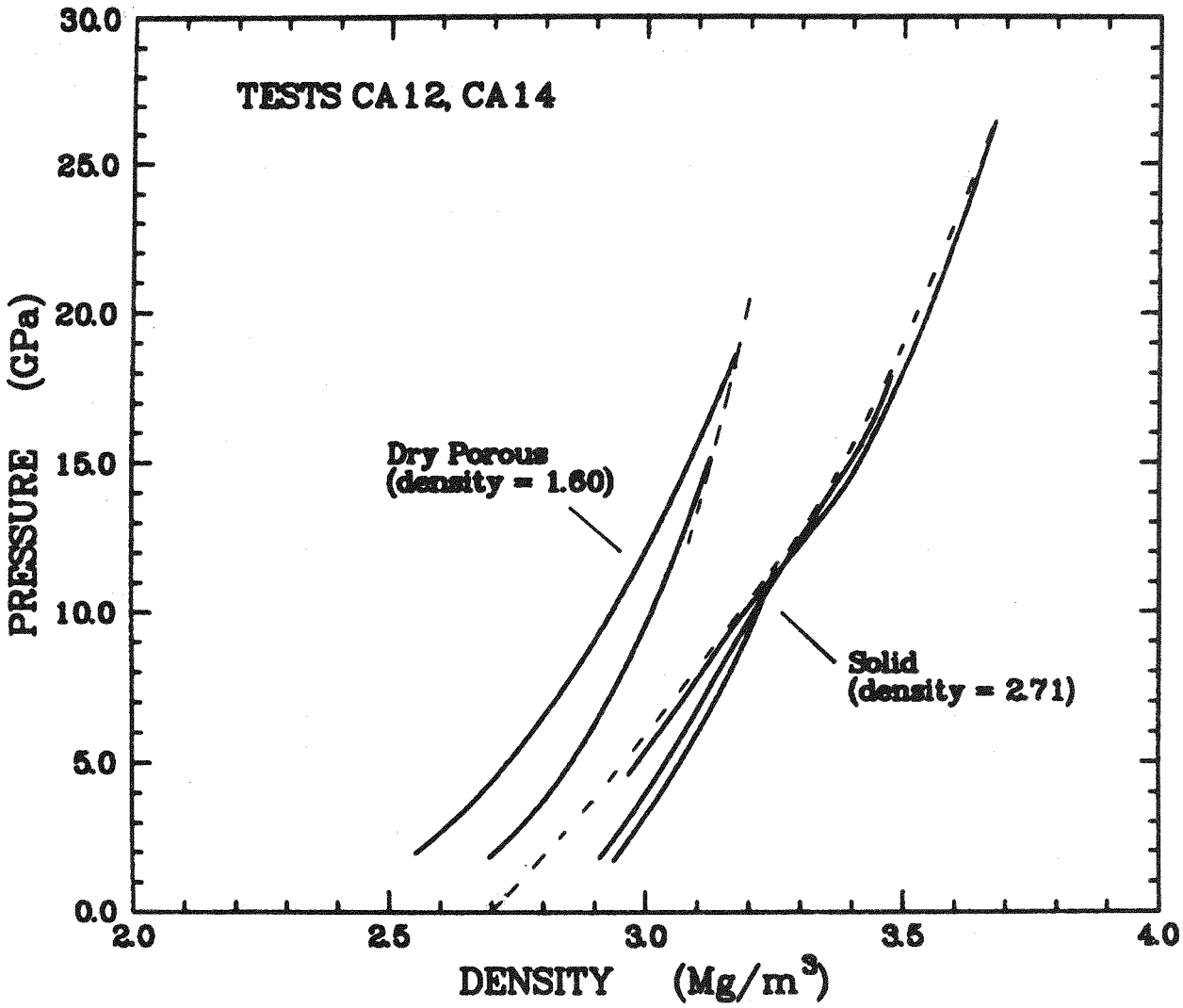

Figure 11: Release paths (solid lines) for 1.60 Mg/m^3 initial density dry-porous calcite measurements. Dashed lines represent Hugoniot states.

epoxy bonded in place (see Figure 8) to insure that no water was lost during evacuation of the target chamber during preparation for the impact environment.

4.2.8 Experiments on Dry and Water-Saturated Porous Calcite

A series of six experiments were successfully completed on dry and water-saturated porous calcite. The target configuration was identical to that shown in Figure 8 with a LiF window material. Again, a small buffer was used between the window and calcite. In this case, aluminum was used for the buffer material because it is a good impedance match for LiF. The data for this series of experiments are provided in Table 3. Measured wave profiles are shown in Figures 12-17.

TABLE 3
Data for High-Shock-Pressure Impact
Experiments on Dry and Water-Saturated
Porous Calcium Carbonate

Shot #	State	Density* (kg/m^3)	Impact Velocity (km/s)	Impactor** Thk. (mm)	Stand-off** Thk. (mm)	Sample Thk. (mm)	Buffer** Thk. (mm)	Window*** Thk. (mm)
CA-16	(dry)	1381	3.35	2.236†	0.995	2.162	0.142	17.067
CA-17	(dry)	1352	3.53	2.240	0.961	2.203	0.143	17.189
CA-18	(dry)	1373	4.64	2.237	1.013	2.172	0.138	17.181
CA-19	(wet)	1178 (1744)	3.53	2.018	1.051	2.499	0.136	19.042
CA-20	(wet)	1232 (1777)	4.42	2.018	1.058	2.387	0.140	19.744
CA-21	(wet)	1210 (1760)	5.57	2.006	1.055	2.438	0.143	19.745

*This is the density of drycalcite; number in parenthesis is the wet density.
**6061-T6 aluminum.
***Lithium fluoride.
†One-mm void gap behind impactor plate (see Figure 9).

4.3 Analysis of Dry and Water-Saturated Porous Calcite Experiments

An array of three pins, as shown in Figure 8, provided an electrical time-of-arrival fiducial as the shock wave passed through the aluminum stand-off plate and into the calcite sample (Konrad and Moody, 1986). This signal triggered a light diode which placed an optical fiducial on the photomultiplier tubes used to record the laser interferometer velocity record. By this method, a shock transit time and, hence, shock velocity across the calcite sample was determined. In the development phase of the experimental technique it was recognized that because of the small sample thickness needed to perform release wave measurements, timing errors would be easily accumulated due to both construction and measurement precision requirements. In this series of tests, an accuracy of approximately $\pm 5\%$ in the shock velocity is estimated. With care, the accuracy of such experiments could be improved in future tests.

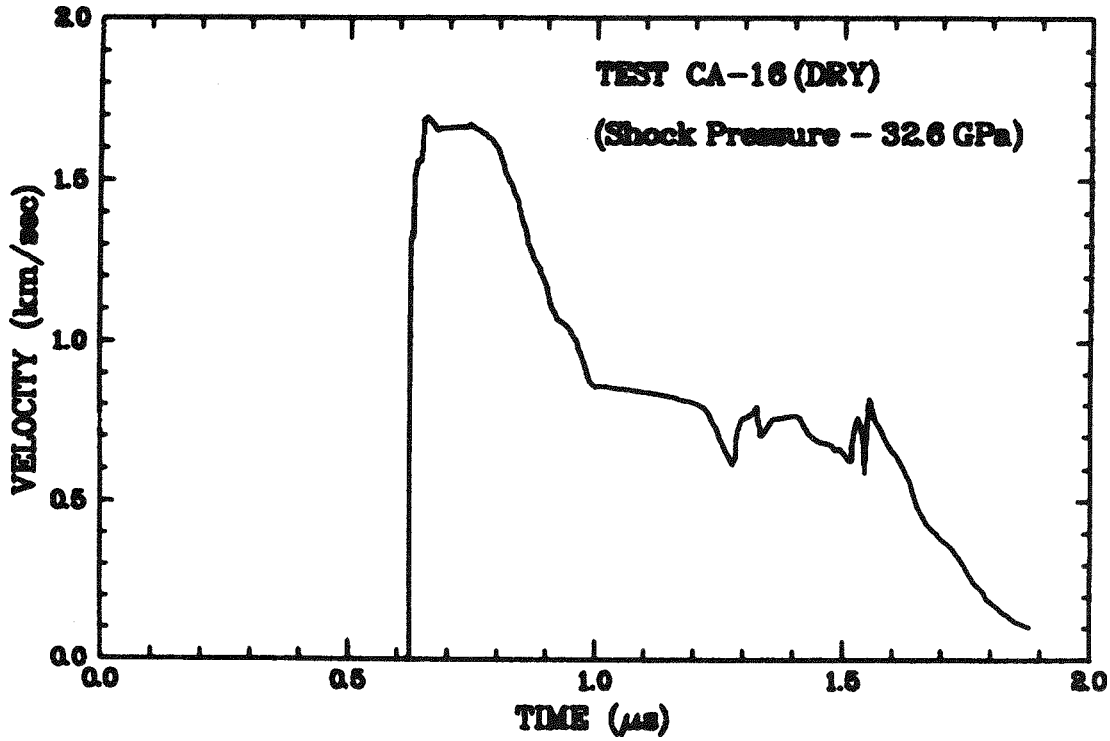

Figure 12: CA-16 wave profile.

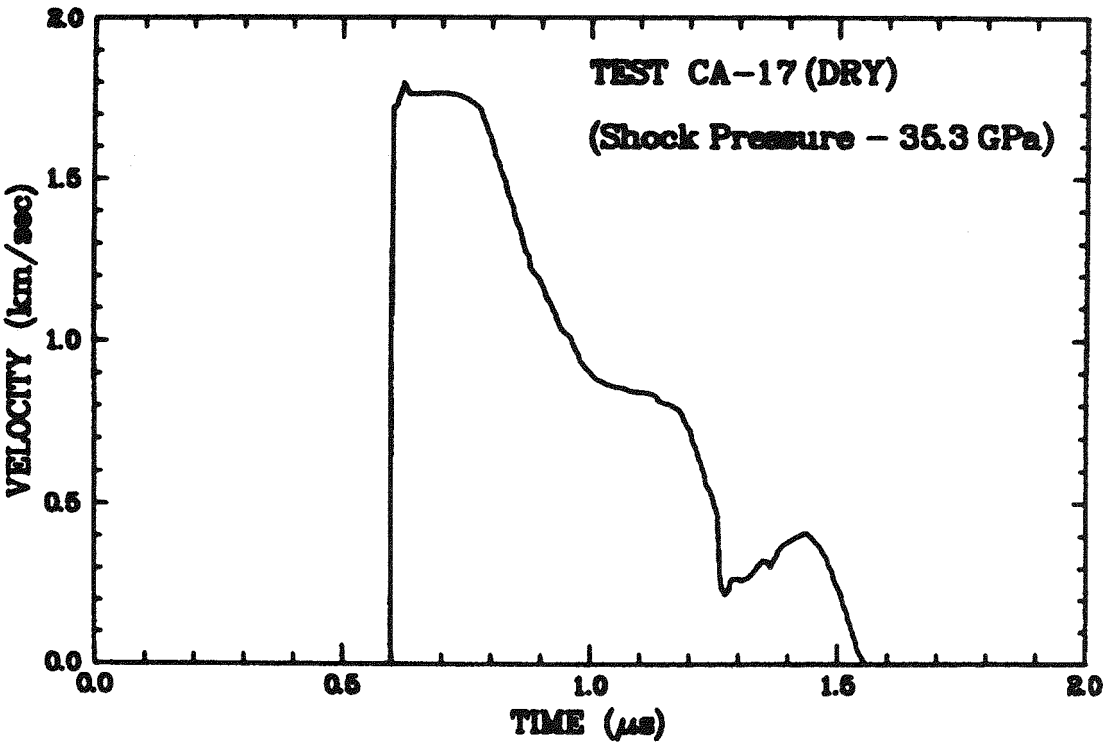

Figure 13: CA-17 wave profile.

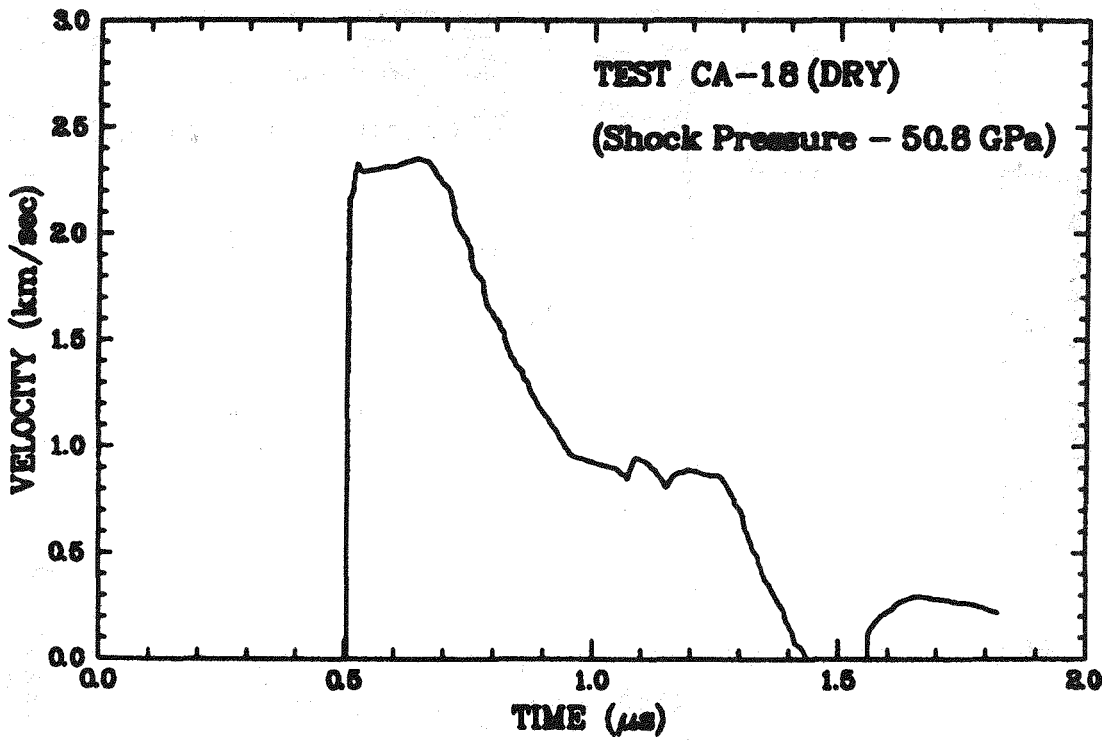

Figure 14: CA-18 wave profile.

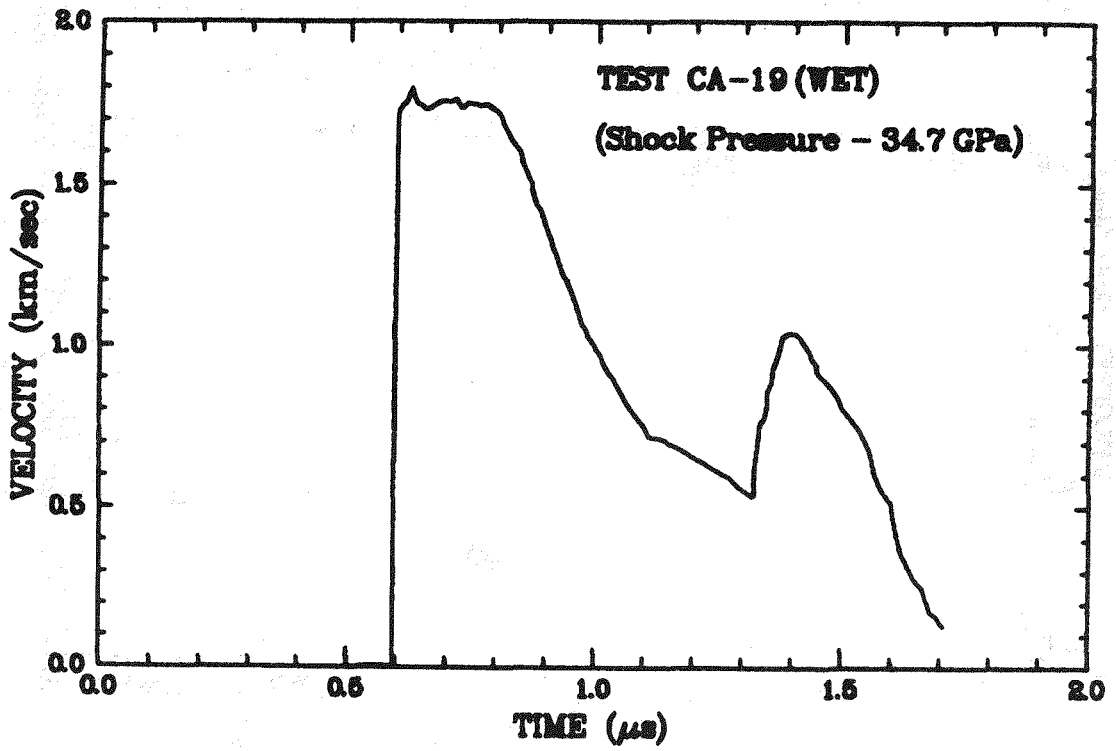

Figure 15: CA-19 wave profile.

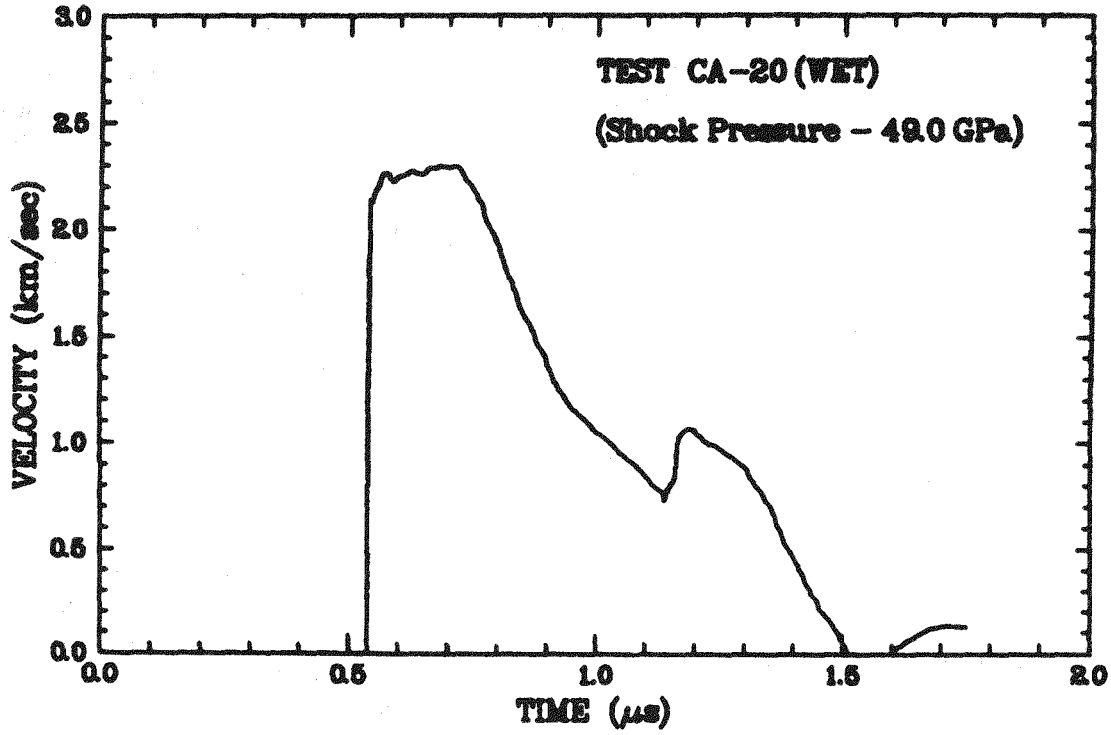

Figure 16: CA-20 wave profile.

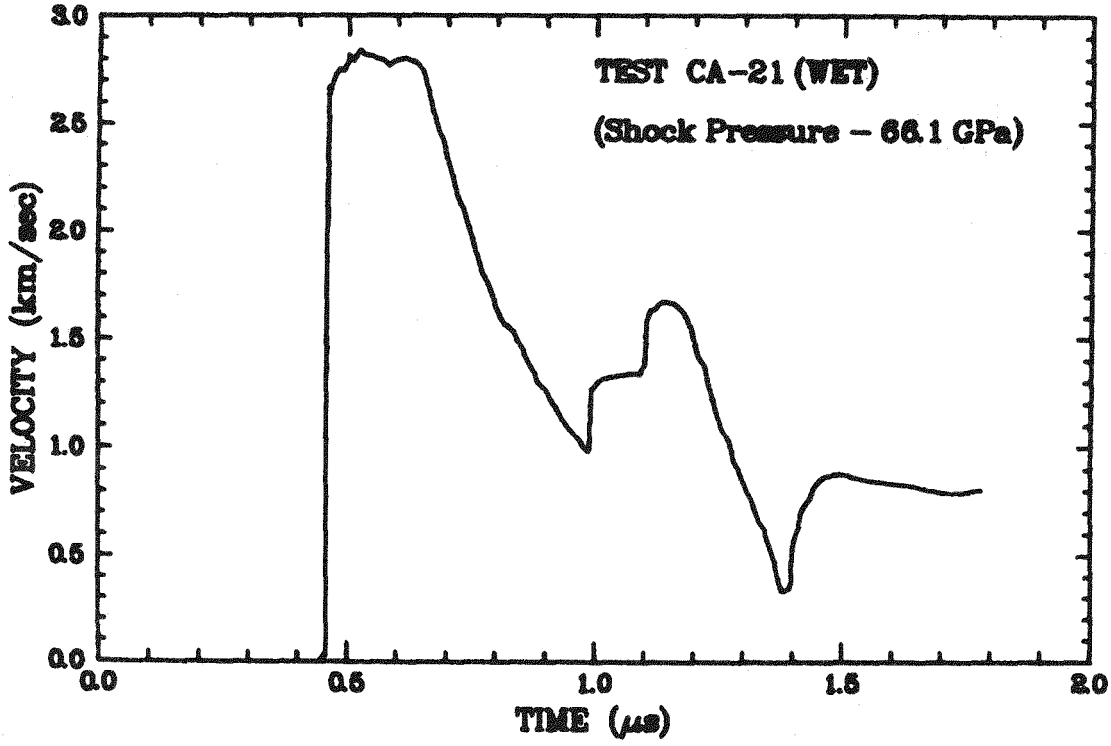

Figure 17: CA-21 wave profile.

The particle velocity in the calcite is calculated from the intercept of the calcite Rayleigh line, as determined from the measured shock velocity and the aluminum Hugoniot in a pressure-particle velocity plot. The shock velocity-particle velocity data for the first shock state are shown in Figure 18 for dry-porous calcite and in Figure 19 for the water-saturated calcite. The data are also compared with measurements of other authors.

The second or reflected shock state is readily calculated from the maximum particle velocity level determined from the measured wave profiles in Figures 12 through 17, and the known pressure-particle velocity Hugoniot for lithium fluoride. Both the initial and reflected shock states for experiments CA-16 through CA-21 are shown in Figures 20 and 21. The aluminum Hugoniot determines the states of the impact material, with the zero pressure intercepts corresponding to the projectile velocity in each experiment

Calculation of pressure-density release paths in the present series of experiments is based on a computation of the impact particle velocity profile at the interface between the aluminum stand-off plate and the calcite sample. This computation was performed with a one-dimensional stress wave code which calculated the complete impact problem using a thermodynamic equation of state for the aluminum and lithium fluoride, and a mixture model for the dry and water-saturated porous calcite. The theoretical basis for this calculation is discussed in the following section. Although the accuracy of the interface profile is dependent on the reliability of the aluminum equation of state, aluminum has been well characterized and the model is believed to be sufficiently accurate for the present purpose.

A calculated interface profile is shown in Figure 22, along with the corresponding experimental particle velocity profile. The discontinuous release in the middle of the falling portion of the interface profile corresponds to the arrival of the reflected shock at the stand-off plate-calcite interface. When this is subtracted from the profile, unloading wave velocities across the calcite sample can be determined, and pressure-density release paths can be calculated by the methods of Lagrangian analysis. Note that the calculated arrival of the reflected shock at the interface at the same time as the release from the impact plate free surface attest to adequacy of the experimental design for putting the calcite sample at the reflected shock state prior to arrival of pressure release from the impact plate.

The two profiles are aligned in time through the measured initial shock transit time across the calcite sample. This determines the time separation between the shock arrivals in the two profiles in Figure 22.

4.4 Pressure-Density Release Paths for Dry and Water-Saturated Porous Calcite

Release paths for the dry-porous calcite experiments are shown in Figure 23 and compared with the solid calcite Hugoniot and the porous Hugoniot based on the measured first shock states. Similar release paths for wet porous calcite are shown in Figure 24. The middle release path corresponds to test CA-20 and is suspect due to the low measured shock velocity. We note that a shock velocity consistent with CA-19 and CA-21 would also bring the slope of the release path into consistency. The release data for both wet and dry porous calcite are compared in Figure 25 to illustrate differences in behavior.

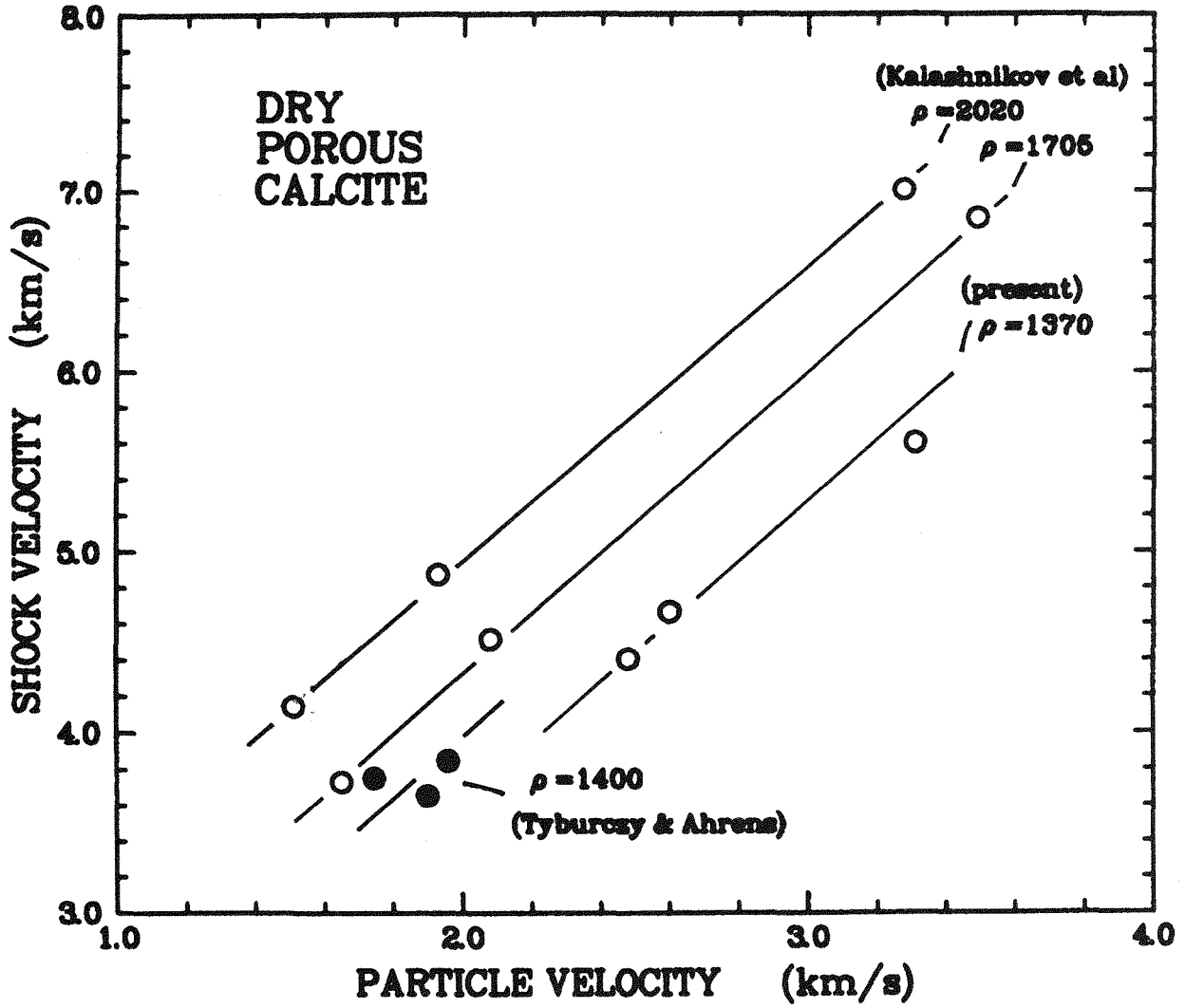

Figure 18: Shock velocity-particle velocity data for dry porous calcite.

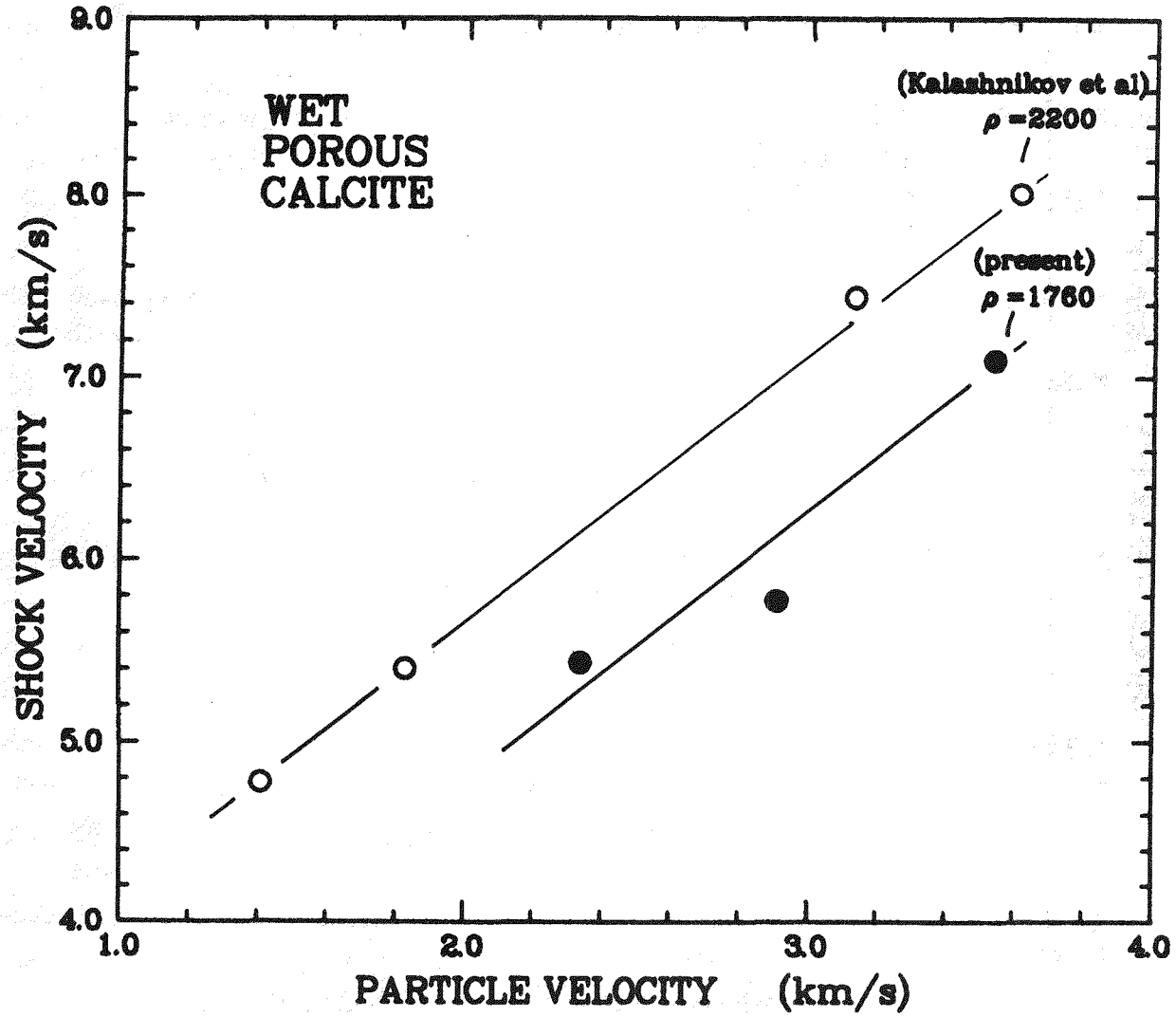

Figure 19: Shock velocity-particle velocity data for water-saturated porous calcite.

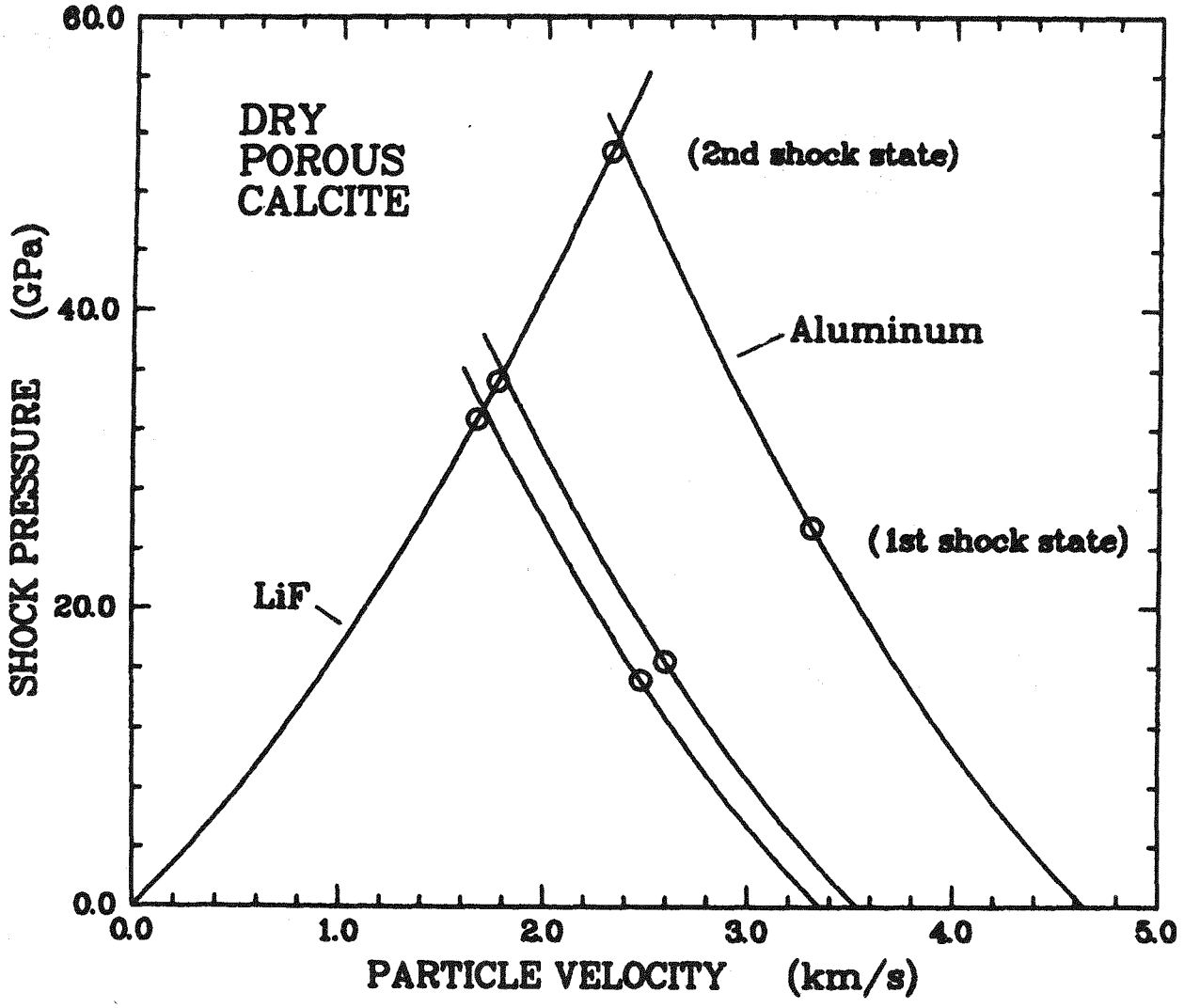

Figure 20: Pressure-particle velocity plot showing first shock and reshock states for dry porous calcite experiments (CA-16, 17, 19.)

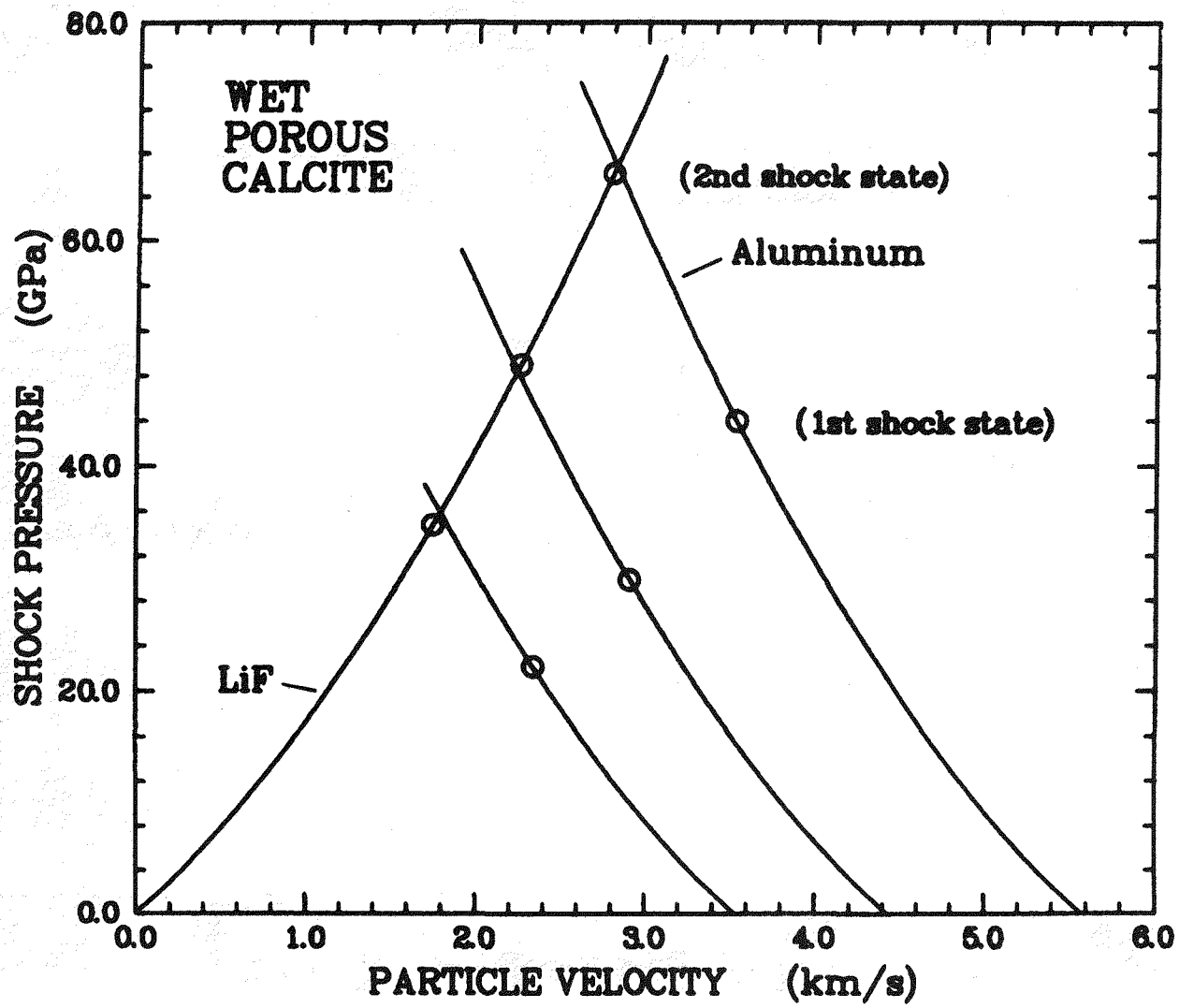

Figure 21: Pressure-particle velocity plot showing first shock and reshock states for water-saturated calcite experiments (CA-19, 20, 21).

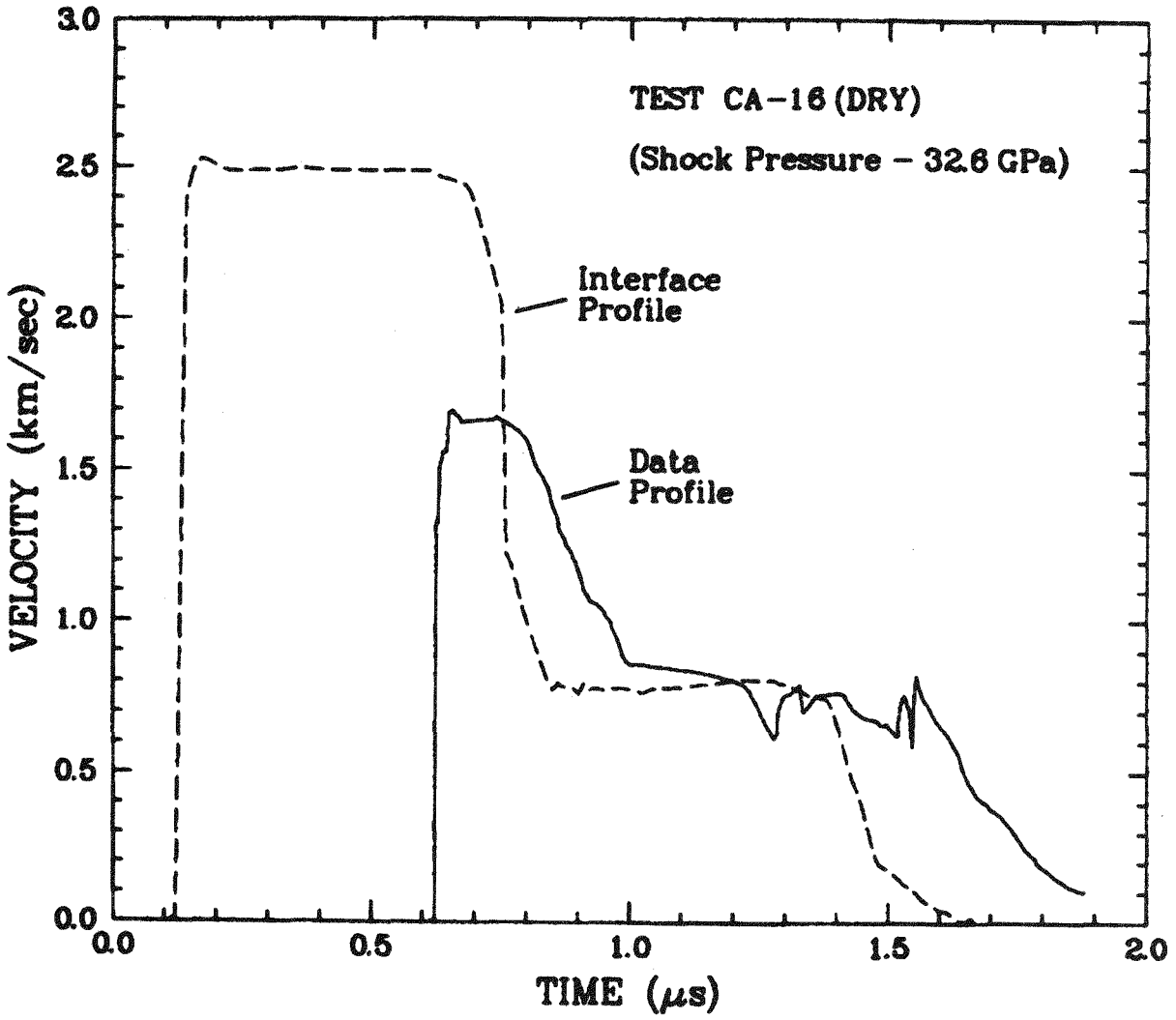

Figure 22: Calculated interface profile and data profile for experiment CA-16 illustrating method for obtaining pressure-volume release states.

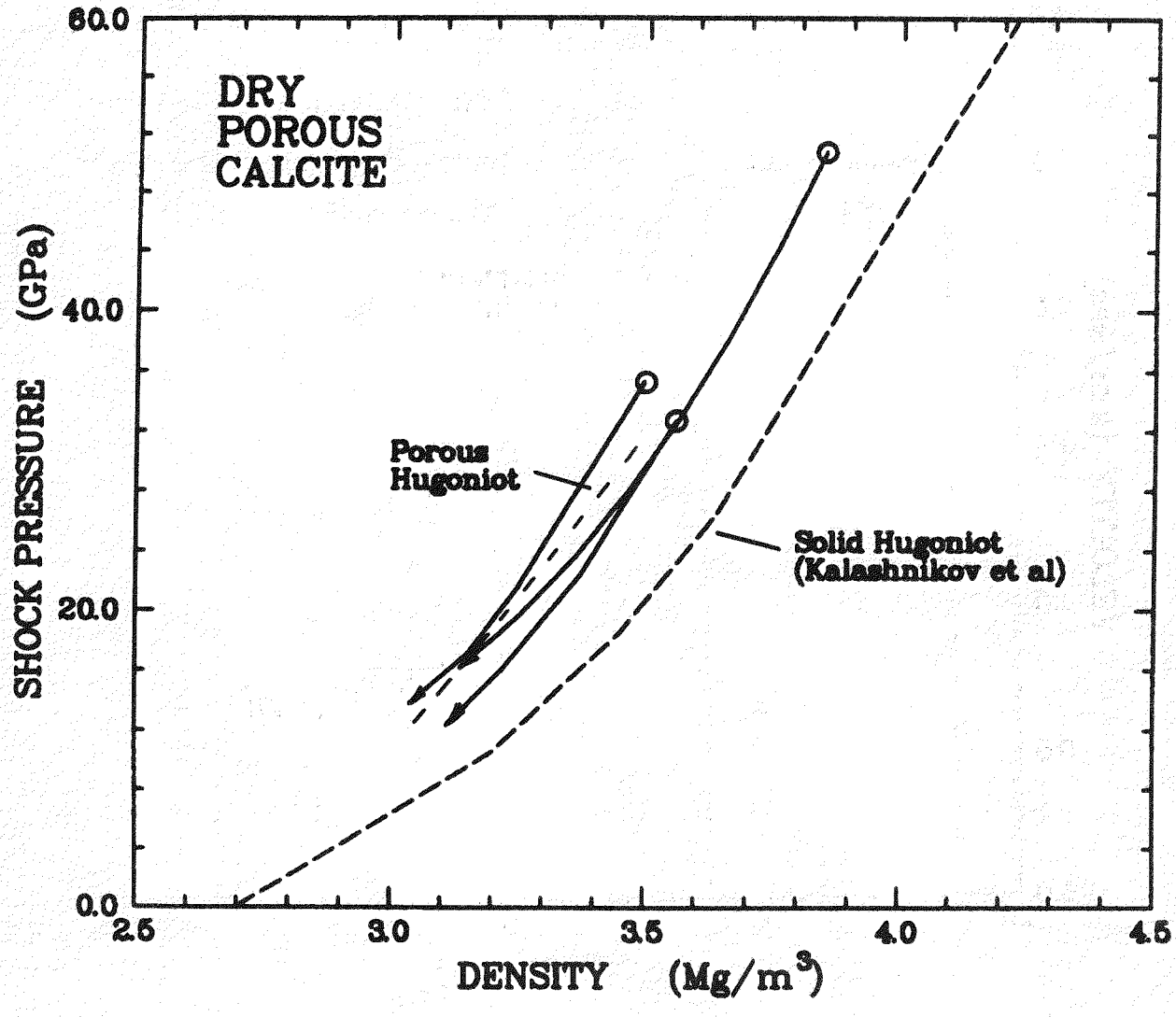

Figure 23: Experiments CA-16, 17, 18. Dashed line shows Hugoniot segment measured for first shock states. Circles and solid lines represent second shock states and release paths.

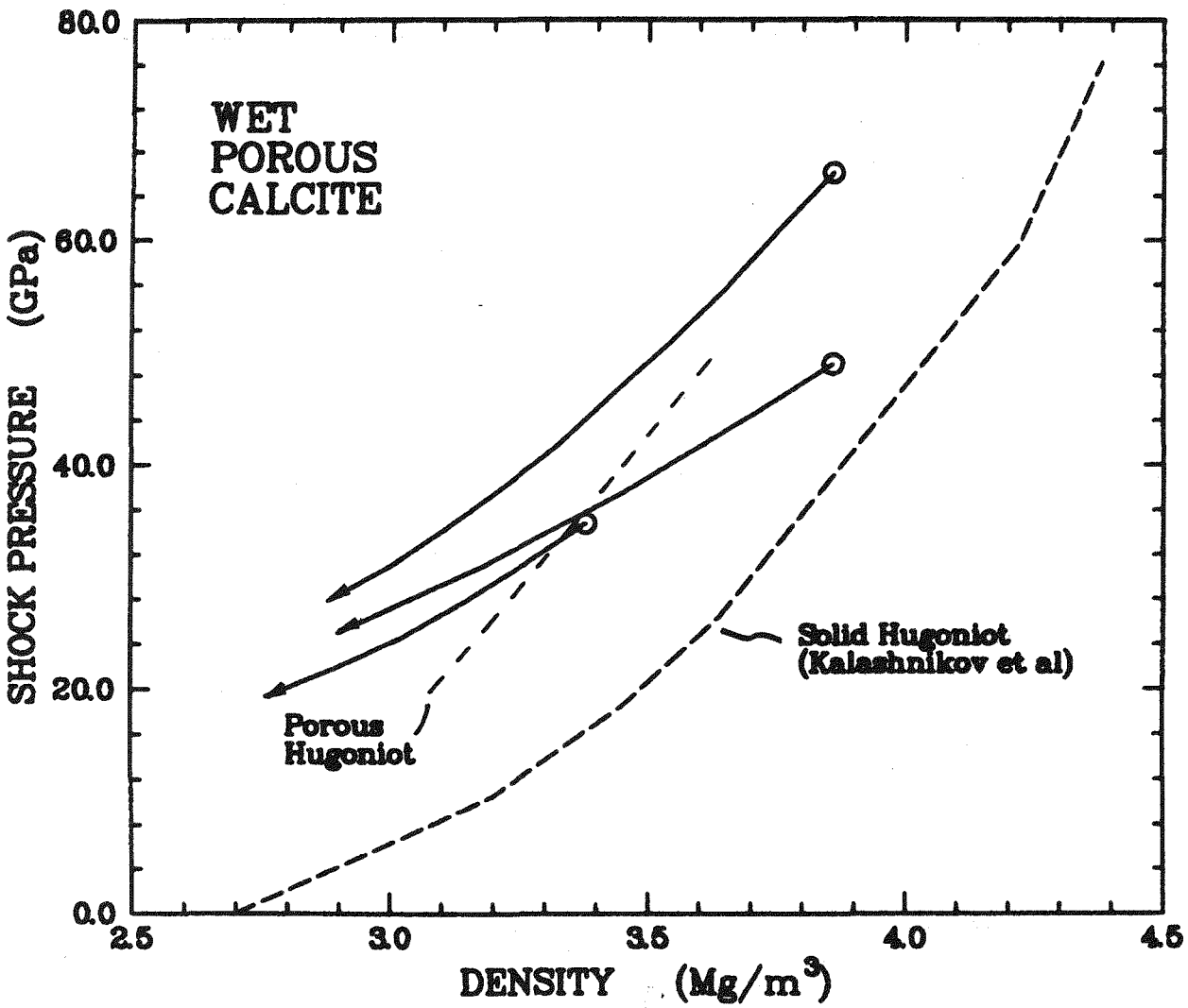

Figure 24: Experiments CA-19, 20, 21. Dashed line shows Hugoniot segment measured for first shock state. Circles and solid lines represent second shock states and release paths.

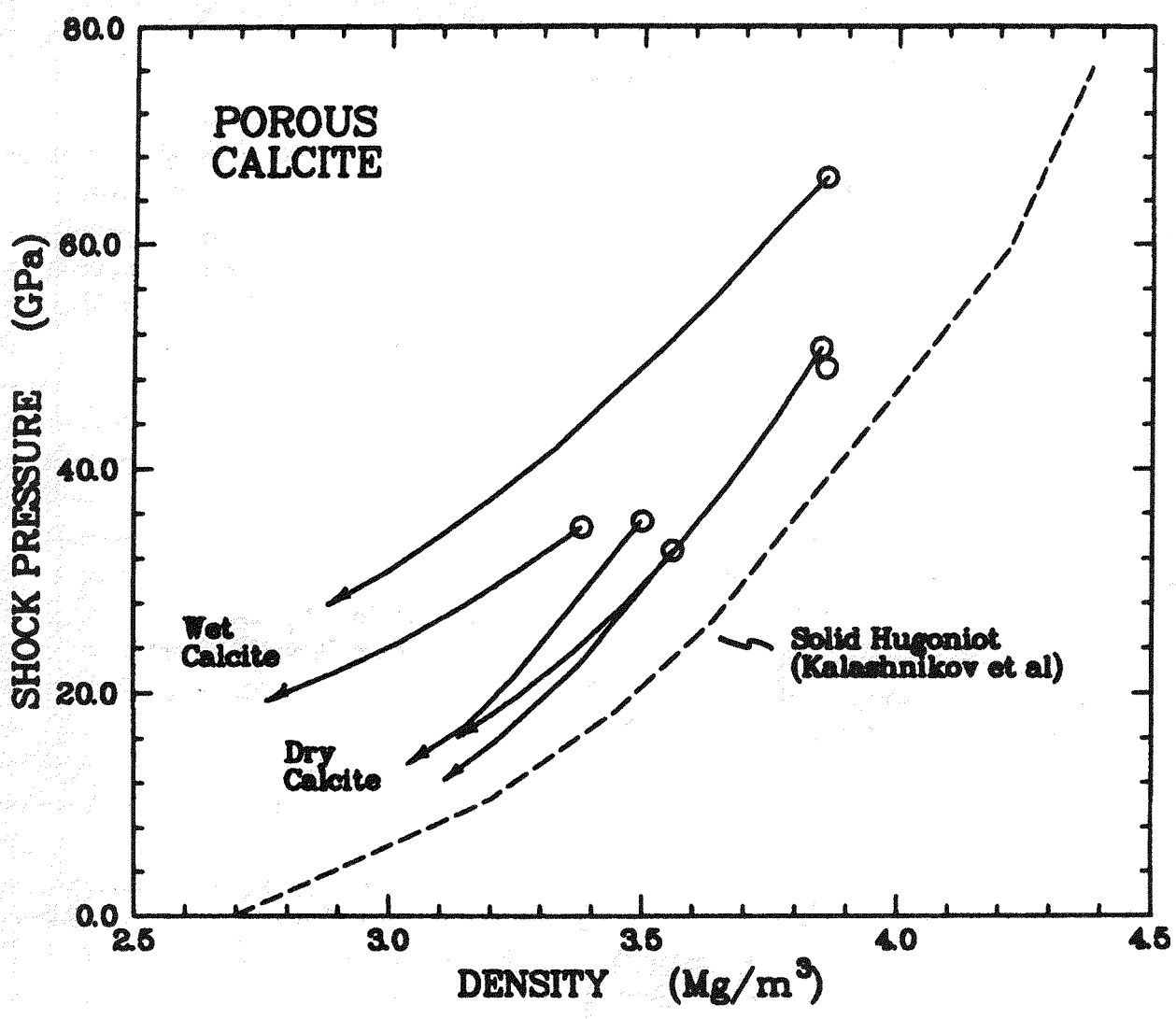

Figure 25: Release paths from double shock states for wet and dry porous calcite experiments.

5 EQUATION-OF-STATE MODELING OF POROUS CALCITE

5.1 Background

Two forms of calcite have been studied in this work, crystalline calcite and porous calcite. The crystalline material exhibits phase transitions which greatly complicate its shock wave response. The porous material does not clearly exhibit these phase transitions; however, other factors complicate the response. In the dry calcite samples, 50 percent of the material volume is void. Since the strength of the lattice formed by the grains of calcite is negligibly small in comparison to the impact loads imposed during these experiments, the void is crushed out of the samples during loading. It is the nature of shock-wave loading that large dissipational stresses accompany this compaction process. This results in enormous temperature increases within the samples; that is, on the order of 5000 to 10,000 $^{\circ}K$. Two things contribute to the production of these temperatures; the formation of a structured shock wave within the loaded sample, and the low crush strength of the sample.

When water is introduced into the pores of the powder samples, crushing is inhibited. However, due to the relatively high compliance of water when compared to the calcite grains, significant crushing still occurs and a large amount of heating is still produced. As with the dry samples, the total energy dissipated by the shock wave within the water-calcite mixture can be determined theoretically. Unfortunately, the theory does not reveal how this energy is partitioned between the water and calcite. It is important to note that this is not a question of thermal conduction or radiation between these two constituents, but rather a question of how the passing shock wave directly deposits its energy within each of the constituents.

The theory described in the following section treats the powdered calcite as an immiscible mixture; that is, an agglomerate of either calcite granules and water (wet samples) or calcite granules and void (dry samples). This mixture theory is described in detail by Drumheller and Bedford (1980). It has been applied to other problems which are similar to the present work; specifically, to calculate the response of partially saturated ashfall tuff (Drumheller, 1986) where it has proven extremely useful for prediction of in-situ stress gage records and cavity volumes created by underground explosions.

Four constitutive elements are present in this theory; the equation of state of calcite, the equation of state of water, the mechanical mixing rule, and the thermal mixing rule. The equation of state for calcite is a Mie-Grüneisen formulation with parameters determined from the shock-wave data of Kalashnikov, *et al.* (1973) and the release-wave data contained in this work. The equation of state for water is a tabular formulation given by Kerley (1985). These two constitutive elements are fixed throughout all of the calculations presented in this work; for example, the equation of state of calcite is not altered by the presence or absence of water.

The third constitutive element, the mechanical mixing rule, is a description of how the shock load is partitioned between the calcite and the water. In this case, the low crush strength of the powder along with the high shock loads suggest that each constituent behaves as a fluid and experiences an equal pressure. More modest shock loads, which are not capable of completely crushing the calcite powder, produce unequal pressures in the two constituents. The lattice formed by the powder then experiences a higher load then the water. The mechanical mixing rule used in this work accounts for this possible pressure difference in that it treats the crushing

of the calcite powder. The theory from which this work is derived also treats general three-dimensional stress states including both Coulomb and von Mises yield behavior and both elastic and plastic dilatancy; however, because of the one-dimensional nature of the experimental data, these phenomena will not be included in the present analysis.

The final constitutive element, the thermal mixing rule, describes how the dissipated shock energy is distributed between the constituents and how thermal energy is conducted and radiated between neighboring constituents. In this work several assumptions for this rule will be made and compared. It will first be assumed that heat conduction and radiation are sufficiently high so as to always produce equal temperatures between neighboring constituents. An alternate assumption is that no thermal energy is exchanged and all of the dissipated energy is deposited in only one of the constituents.

5.2 Theory

Wet calcium carbonate is a mixture of three constituents, solid calcium carbonate, water, and void. It is modeled by using a theory of immiscible mixtures proposed by Drumheller and Bedford (1980). The reader is referred to that work for a more complete description of this theory. In addition, Drumheller (1986) describes an application of this theory to a problem which is similar to the present one. In this section only a brief outline of the theory will be presented.

To facilitate the present discussion, the solid calcite constituent of the mixture will be referred to as $\mathcal{C}_s$. The subscripts f and v will be used when referring to the water and the void. When a generic reference is made to a constituent the subscript ξ will be used. For example, the intrinsic mass density of $\mathcal{C}_\xi$, is denoted as $\bar{\rho}_\xi$. It is the ratio of the mass of $\mathcal{C}_\xi$ divided by the portion of the mixture volume occupied by $\mathcal{C}_\xi$. The volume fraction of $\mathcal{C}_\xi$, is denoted as ϕ_ξ. It is the ratio of the volume occupied by $\mathcal{C}_\xi$ over the volume occupied by the mixture. Since these three constituents comprise the total volume of the mixture, the ϕ_ξ always satisfy the condition

$$\sum \phi_\xi = 1 \quad , \tag{5.1}$$

where the summation sign implies a sum over all constituents $\mathcal{C}_\xi$. The partial mass density of $\mathcal{C}_\xi$ is denoted by ρ_ξ and is given by

$$\rho_\xi = \phi_\xi \bar{\rho}_\xi. \tag{5.2}$$

In situations where the $\mathcal{C}_\xi$ have independent motions, balance of mass and momentum equations are required for each constituent. In this analysis it is assumed that all the $\mathcal{C}_\xi$ are restricted to the same one-dimensional motion. As a result only one balance of mass and one balance of momentum relation are required. These relations are identical to the traditional continuum relations in which the density ρ and the pressure P are identified with the mixture mass density $\rho = \sum \rho_\xi$ and the effective mixture pressure.

The effective mixture pressure is comprised of several parts. These terms can be grouped into two general categories, equilibrium and dissipative. Since this work treats shock loading of porous materials, inclusion of the dissipative terms is central to the development of the model. The equilibrium components of the pressure within each constituent will be denoted as P_ξ, and the dissipative pressures will be denoted as Q_ξ. The effective mixture pressure in terms of these components is then

$$P = \phi_s(P_s + Q_s) + \phi_f(P_f + Q_f). \tag{5.3}$$

Specific constitutive relationships for these terms will be discussed later. Because of the effects of large dissipational loads, these constitutive relations will depend on the specific internal energies E_ξ of the water and the calcite. Therefore, balance of energy relations are required in the analysis.

The specific internal energy of the mixture E, is given by

$$\rho E = \sum \rho_\xi E_\xi. \tag{5.4}$$

It obeys the balance of energy equation for the mixture

$$\rho \dot{E} = P \frac{\dot{\rho}}{\rho} \tag{5.5}$$

where the dot denotes a material derivative and for simplicity the specific external heat supply has been omitted.

When water is present in the pores of the calcite, an additional balance of energy equation is required. The balance of energy equation for the water is

$$\rho_f \dot{E}_f = \phi_f (P_f + Q_f) \frac{\dot{\bar{\rho}}_f}{\bar{\rho}_f} + \epsilon_f \tag{5.6}$$

where ϵ_f denotes the thermal energy exchange from the water to the neighboring calcite. One of two assumptions will be made for this term. Either an adiabatic wall exists between the water and the calcite so that $\epsilon_f = 0$, or the conduction and radiation is very large so that Equation 5.6 can be replaced by the temperature condition $T_f = T_s$. These two assumptions will be called the adiabatic and isothermal mixing assumptions.

To complete the theory, specific constitutive relations are required for the expressions P_ξ and Q_ξ. Two special cases will be considered, wherein the strength due to intergranular contact is first ignored and then included.

If the strength of the calcite powder resulting from the intergranular contact is ignored, the wet or dry powder can only sustain a finite void volume under dynamic loading conditions or under static no-load conditions. For equilibrium conditions, the pressures within the calcite and the pore water must be equal. It is assumed that under dynamic conditions, large differences can exist between the Q_ξ; however the condition $P_s = P_f$ will still apply. The relations for the equilibrium pressures for each constituent are given by conventional thermodynamic equations of state.

It is assumed that C_s has an equilibrium pressure given by the Mie-Grüneisen relation

$$P_s = \frac{\bar{\rho}_{s0} c_{s0}^2 \eta_s}{(1 - s_s \eta_s)^2} \left[1 - \frac{1}{2} \Gamma_{s0} \eta_s \right] + \bar{\rho}_s \Gamma_s e_s \quad , \tag{5.7}$$

and

$$\bar{\rho}_s \Gamma_s = \bar{\rho}_{s0} \Gamma_{s0} \left(1 - \eta_s \right)^n \quad , \tag{5.8}$$

where $\eta_s = 1 - \bar{\rho}_{s0}/\bar{\rho}_s$ and e_s is the specific internal energy. The material constants $\bar{\rho}_{s0}$, c_{s0}, Γ_{s0}, and n are properties of the calcite mineral. A variable Grüneisen parameter Γ_s is assumed ($n = 0$ corresponds to the common assumption that $\bar{\rho}_s \Gamma_s = \bar{\rho}_{s0} \Gamma_{s0}$). Equation 5.8 is equivalent to that proposed by Al'tshuler, *et al.* (1958).

The C_f has an equilibrium pressure given by a tabular equation of state (Kerley, 1985) based on Hugoniot data for water to 100 GPa.

The expressions for the dissipative pressures, Q_ξ, are based on an artificial viscosity expression found in many numerical wave propagation codes (Kipp and Lawrence, 1981),

$$Q = \rho b_1^2 (\frac{1}{\rho}\frac{\partial \rho}{\partial t})^2 + b_2 (\frac{\partial \rho}{\partial t}) \tag{5.9}$$

where b_1 and b_2 are constants which are adjusted so that this term is only significant during rapid loading rates and not during less rapid release processes.

In numerical calculations such a viscosity term spreads a shock wave over several computational cells to produce a steady propagating structured wave. It is a well known result of nonlinear wave analysis that all steady waves and shock waves satisfying the conservative principle described above require existence of a mechanism to dissipate energy and that the total energy dissipated by the passing of the wave is independent of the constitutive relation representing this mechanism. Thus the vicosity expression given in Equation 5.9 will accurately represent the energy dissipated in the calcite samples by the imposed experimental conditions. While the constitutive relation for the dissipative mechanism does not influence the total energy dissipated, it does influence the computed profile of the shock wave; however, this profile was not resolvable in these experiments. Thus there are no data available upon which to construct a relation to replace Equation 5.9.

Equation 5.9 will be used to represent the total dissipative pressure within the mixture; that is,

$$Q = \phi_f Q_f + \phi_s Q_s. \tag{5.10}$$

If the isothermal mixing rule is assumed, this relation and the requirement that the T_ξ are equal is sufficient to completely define the problem. If the adiabatic mixing rule is assumed, additional information must be specified about one of the Q_ξ. Two limiting cases will be considered. They are either $Q_f = 0$ or $Q_s = 0$. In the first case, all of the dissipated energy is absorbed by the calcite, and in the second case by the water. By comparing results from the isothermal case and the two adiabatic cases, the sensitivity of the model to the form of the thermal mixing rule can be estimated.

The expressions above complete the definition of the model for the case when the influence of intergranular contact is ignored. When the strength of the intergranular contact is included, the pressure in the calcite granules is greater than that in the pore water, and the assumption that $P_s = P_f$ is no longer valid. This assumption is replaced by the following constitutive relation for the pressure difference:

$$\mathcal{F}(\tilde{\phi}_s) = \Omega \quad , \tag{5.11}$$

where

$$\Omega = \frac{P_s - P_f}{\rho_s} \quad , \tag{5.12}$$

where $\tilde{\phi}_s$ denotes the elastic or recoverable change in the volume fraction of the solid.

There are several important points to note about this relation. First, an elastic component of the volume fraction of the calcite is defined. This differs from the previous equal-pressure assumption in which all of the change in ϕ_s is plastic. Next, $\mathcal{F}$ is an arbitrary constitutive relation of the elastic volume fraction of the solid. The functional form of the term Ω is determined

by continuum mechanics principles, specifically considerations about entropy production within the mixture. Normally $\mathcal{F}$ is specified so that an increase in the pressure P_s results in reduction of pore volume; that is, an increase in $\tilde{\phi}_s$. These relations then indicate that an increase in the water pressure will cause an increase in the pore volume of the powder.

When a dry porous solid is considered, $\Omega = P_s/\rho_s$. Equation 5.11 is then simply a relationship between the porosity of the solid and the pressure load on the solid. Relations of this type have been proposed previously, Herrmann (1968), where they have been called $P - \alpha$ relations. It is important to note that the same relation describes the behavior of the solid regardless of whether it is dry or saturated. Because of Equation 5.12, data obtained for dry solids can be applied directly to partially or fully-saturated solids.

The explicit form of Equation 5.11 used in this work is one suggested by Herrmann,

$$\frac{\tilde{\phi}_{sm} - \tilde{\phi}_s}{\tilde{\phi}_{sm} - \phi_{s0}} = \left(\frac{\Omega_m - \Omega}{\Omega_m}\right)^r \quad , \tag{5.13}$$

where $\tilde{\phi}_{sm}$, Ω_m, and r are specified constants. The change in the plastic volume fraction will be controlled by a yield condition. It is required

$$-\Omega_e \leq \frac{P_{sb} - P_s}{\rho_s} \leq \Omega_l \quad , \tag{5.14}$$

where, following the form suggested by Herrmann, Ω_l is given by

$$\left(\frac{\Omega_m - \Omega_l}{\Omega_m - \Omega_e}\right)^2 = \frac{1/\phi_s - 1}{1/\phi_{s0} - 1} \quad . \tag{5.15}$$

The parameters Ω_m and Ω_e are positive constants. It is intended that the same values for Ω_m be used in this relation and in Equation 5.13.

Equations 5.13 and 5.15 are illustrated in Figure 26. In situations when the value of Ω increases and attempts to move the material response outside the envelope formed by Equation 5.15, the plastic volume fraction increases so as to displace the origin of Equation 5.13 to the right and contain the material response within the envelope.

In the following sections, calculations from the theory developed in this section will be presented. The first group of calculations will be obtained from a steady-wave analysis of these equations. Comparisons of the results will be made to the data of Kalashnikov, *et al.* (1973) and to the release wave data obtained in experiments CA-12 and CA-13. Selection of parameters for the equation of state of calcite are based on these comparisons. The effects of the various choices for the thermal mixing rule will also be illustrated. After this, the theory will be compared to the wave profiles obtained from the remainder of the experiments contained in this work. These comparisons are made without any additional adjustments to the model parameters.

5.3 Comparison of the Theory with Hugoniot Data

Both Hugoniot points and adiabatic release paths are computed in this section. The Hugoniot points are obtained from a steady-wave analysis; that is, the solution was assumed to depend only on the factor $\Psi = x - Ut$, where U is the velocity of the wave, x is the spatial

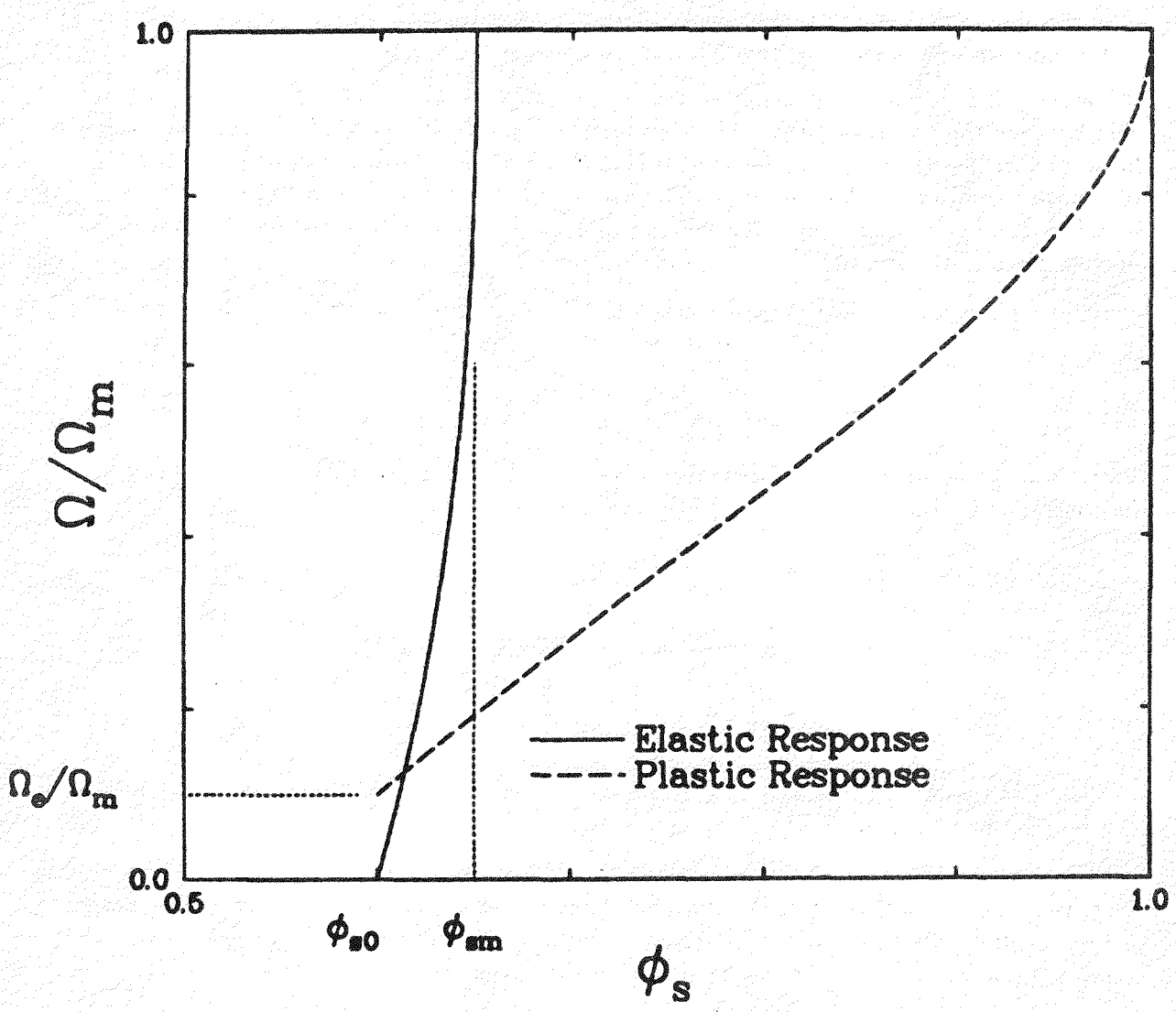

Figure 26: Theoretical Pore-Collapse Behavior.

position, and t is the time. The adiabatic release paths are obtained by integration of the energy equations along an equilibrium path ($Q_\xi = 0$) intersecting the computed Hugoniot point.

The equal-pressure mixing rule and both isothermal and adiabatic mixing conditions are considered. The analysis to obtain these results is standard, albeit tedious, and will not be repeated in this work. For the isothermal case the resulting relations can be analytically integrated to obtain jump conditions for the steady wave. All other results are obtained by numerical integration.

Figure 27 contains comparisons of calculated Hugoniots to the data of Kalashnikov, *et al.* (1973) and Tyburczy and Ahrens (1985) for various initial mass densities. The model parameters used in these calculations are: $\bar{\rho}_{s0} = 2710$ kg/m^3; $c_{s0} = 3.65$ km/s; $\Gamma_s = 0.8$; and $n = -2.25$. The porosities of these samples, which can be computed from the listed initial densities range from zero to approximately fifty percent. With the exception of the water-saturated sample ($\rho_0 = 2200$ kg/m^3), all of these data are for dry chalk. The calculation shown for the water-saturated case corresponds to the isothermal mixing rule.

Good agreement is achieved for the dry samples; however, some discrepancy is observed in the comparison to the water-saturated sample. Kalashnikov, *et al.* (1973) have also proposed a model for water-saturated chalk. They report better agreement for the water-saturated case; however, they do not include a description of their equation of state for water. Additionally, their reported values for mass densities and volume fractions for their saturated sample cannot be reconciled with the standard mass density for water.

The calculated Hugoniot for the water-saturated case is shown again in Figure 28. Also shown are calculations using the two adiabatic mixing rules in which the shock heating is either in the solid or the water. It can be seen that this calculation is relatively insensitive to the choice between the thermal mixing rules for pressures below about 40 GPa. Figure 29 shows the calculated temperatures for these Hugoniots. Here, the specific heat of calcite was assumed to be a constant value of 1200 J/kg K (Dmitriyer, *et al.*, 1972).

Figure 30 shows the corresponding Hugoniot calculations for the wet and dry samples used in this work. Nominal mass densities of 1.76 and 1.38 Mg/m^3 were used. Again, the Hugoniot results are not sensitive to the thermal mixing rule below 40 GPa. The accompanying temperature results for the wet sample are shown in Figure 31. In addition, release path temperatures from a Hugoniot state of 66.1 GPa (Test CA-21) are also illustrated. As with the previous calculations, the porosity of the sample results in very high temperatures, and the values of the temperatures are strongly dependent upon the choice of the thermal mixing rule.

In Figure 32 the calculation is compared with release isentropes obtained from the preliminary shock compression and unloading experiments on dry calcite samples (CA-12,13). Release paths from 15.0 and 18.5 GPa are determined from the measured wave-profile data. The comparison in Figure 32 was used to adjust the volume-dependent Grüneisen parameters used to model the Hugoniot data in Figure 27.

5.4 Comparison of the Theory with Experiments CA-16 thru 21 on Dry and Water-Saturated Porous Calcite.

By a numerical method discussed in detail in Drumheller (1986) the material model described above has been incorporated into a Lagrangian wave-propagation computer code, WONDY

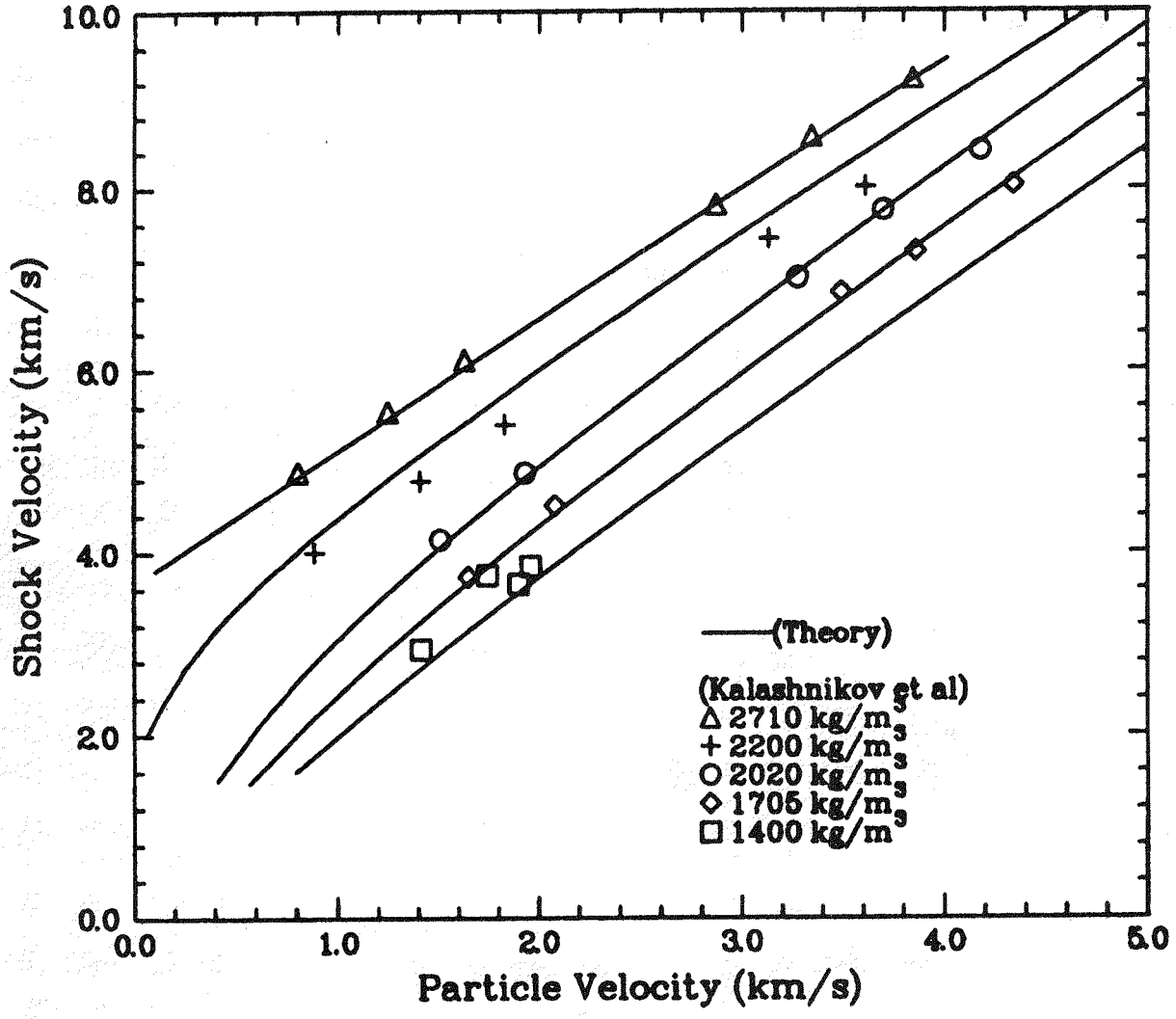

Figure 27: Comparison of Experimental and Theoretical Hugoniot States.

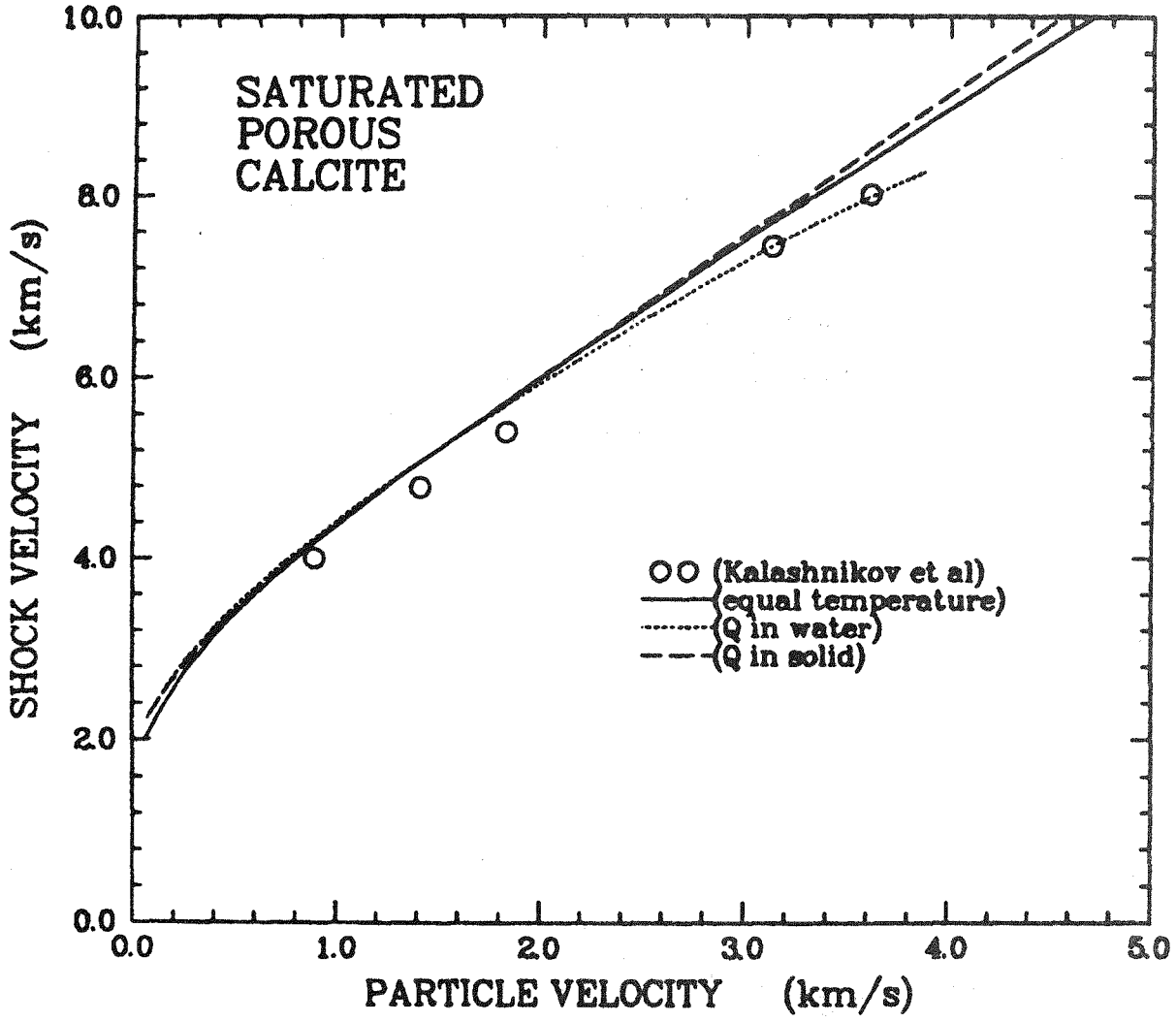

Figure 28: The Influence of the Thermal Mixing Rule on the Theoretical Hugoniot.

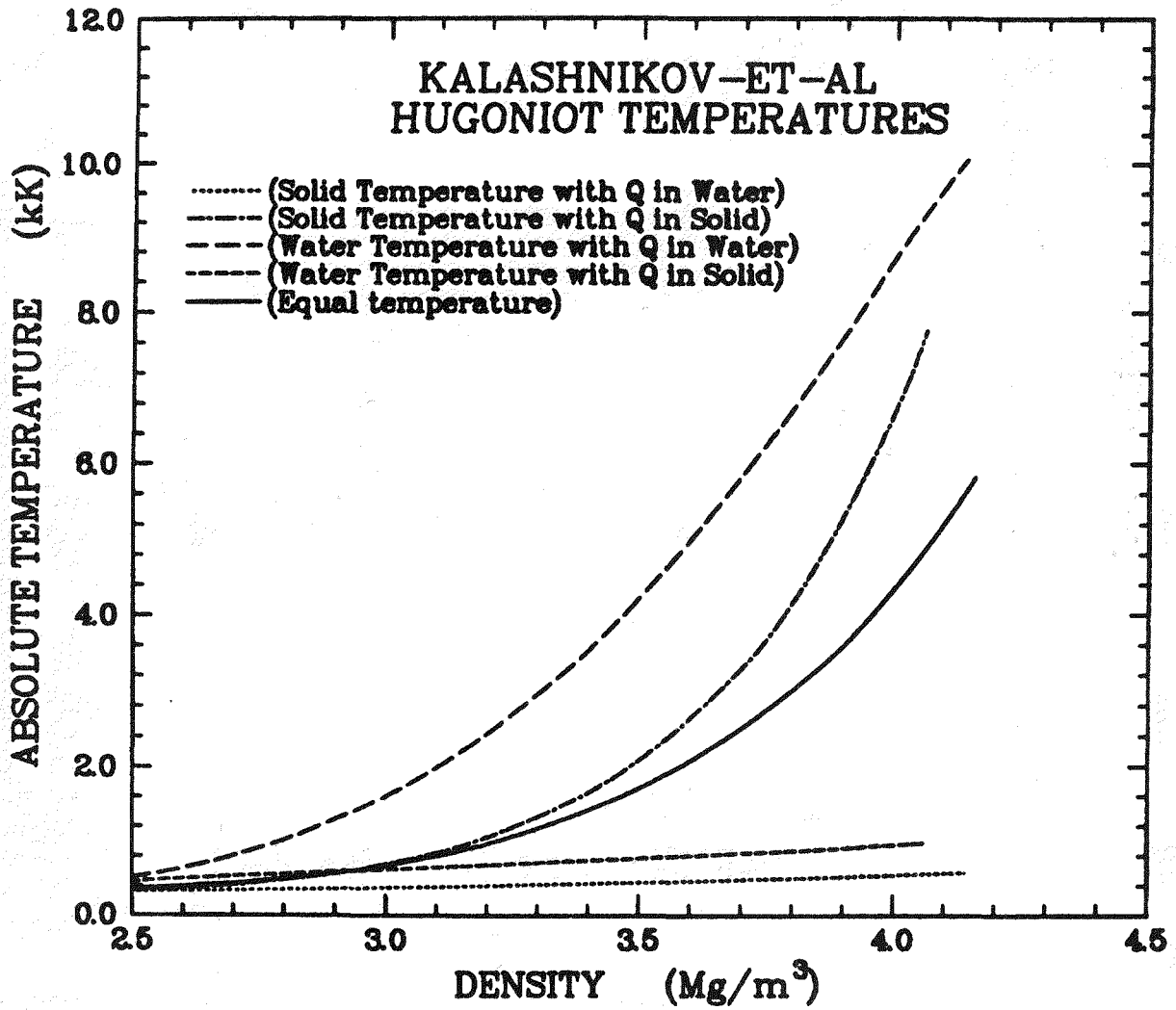

Figure 29: Theoretical Hugoniot Temperatures.

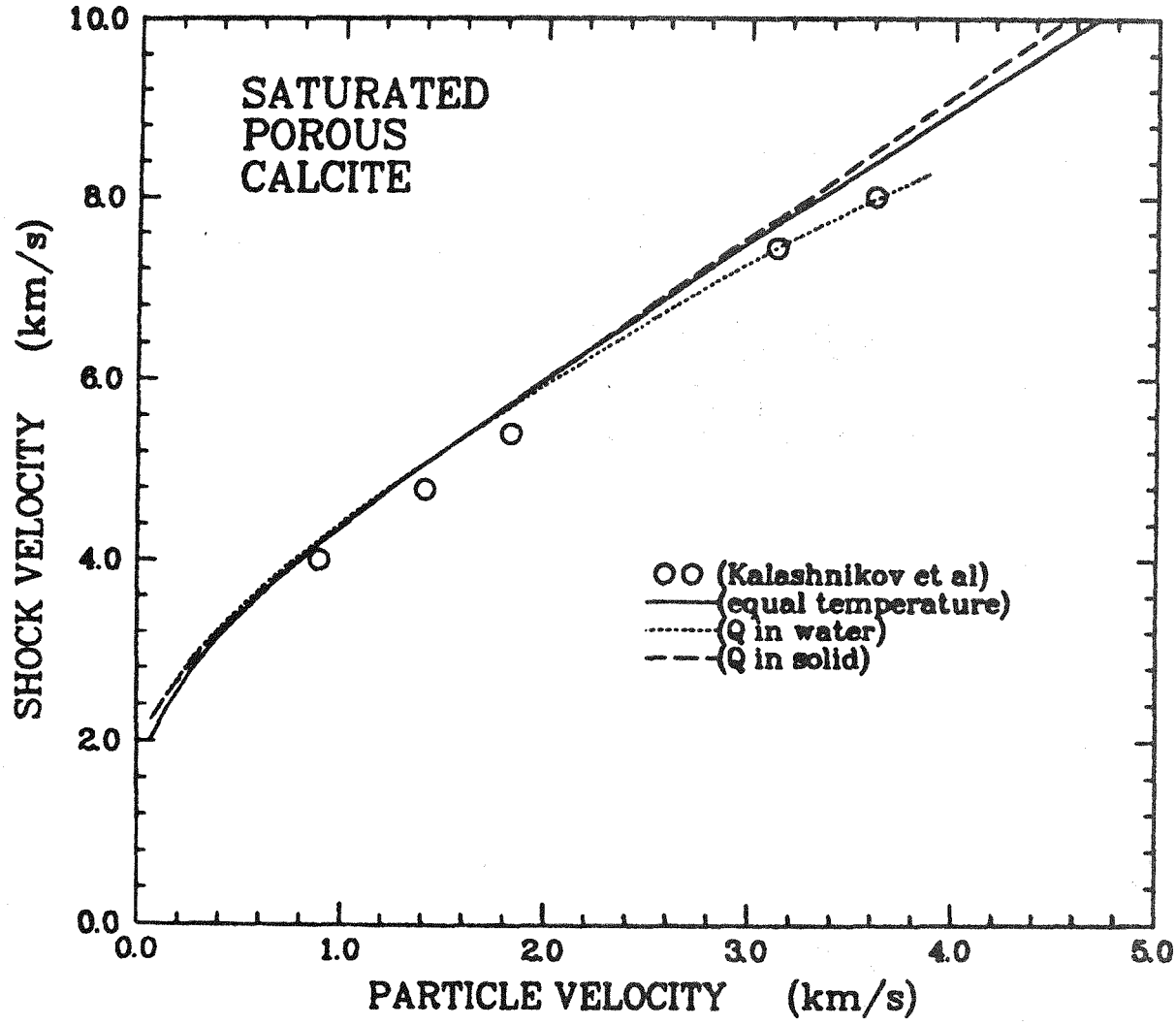

Figure 28: The Influence of the Thermal Mixing Rule on the Theoretical Hugoniot.

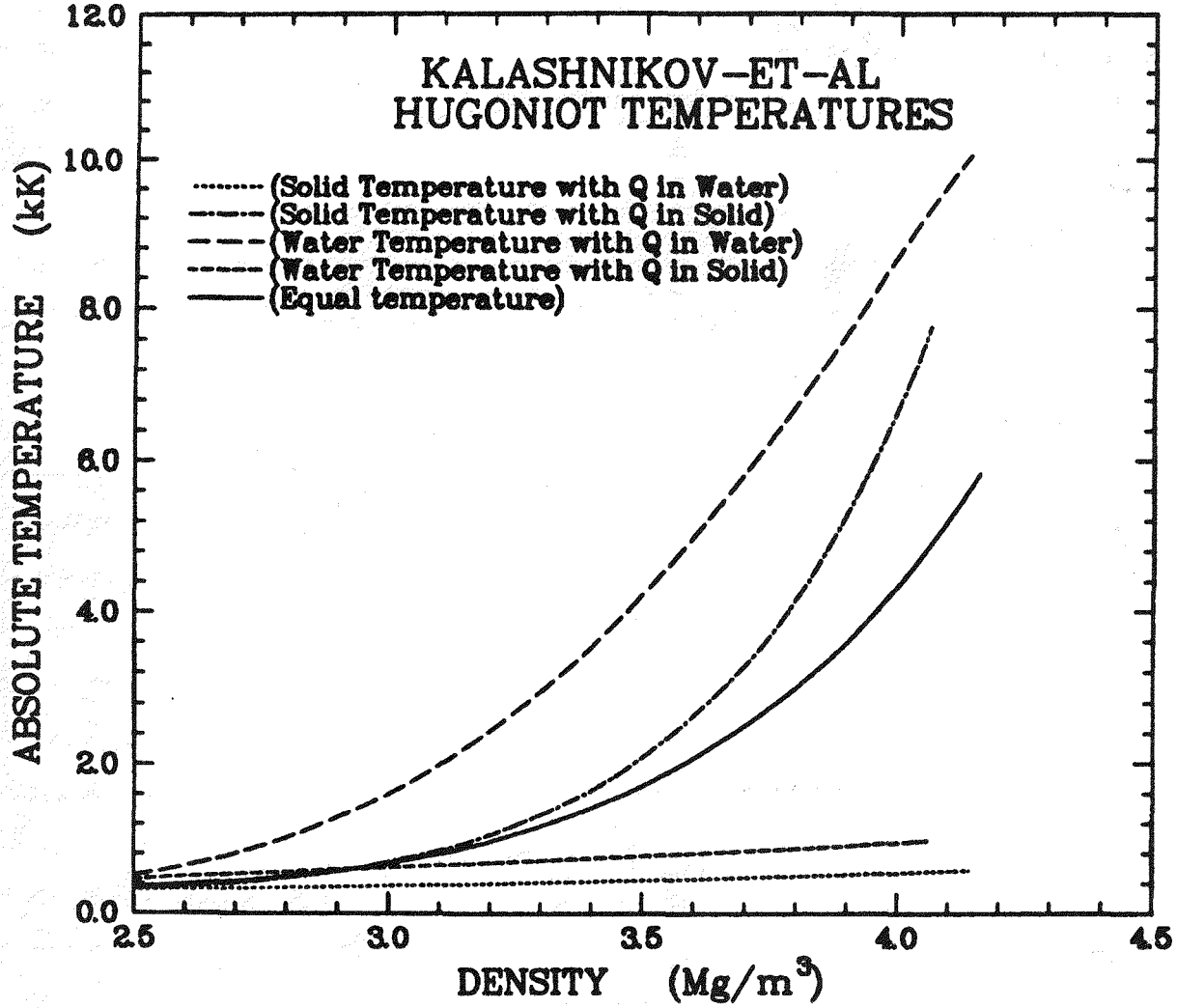

Figure 29: Theoretical Hugoniot Temperatures.

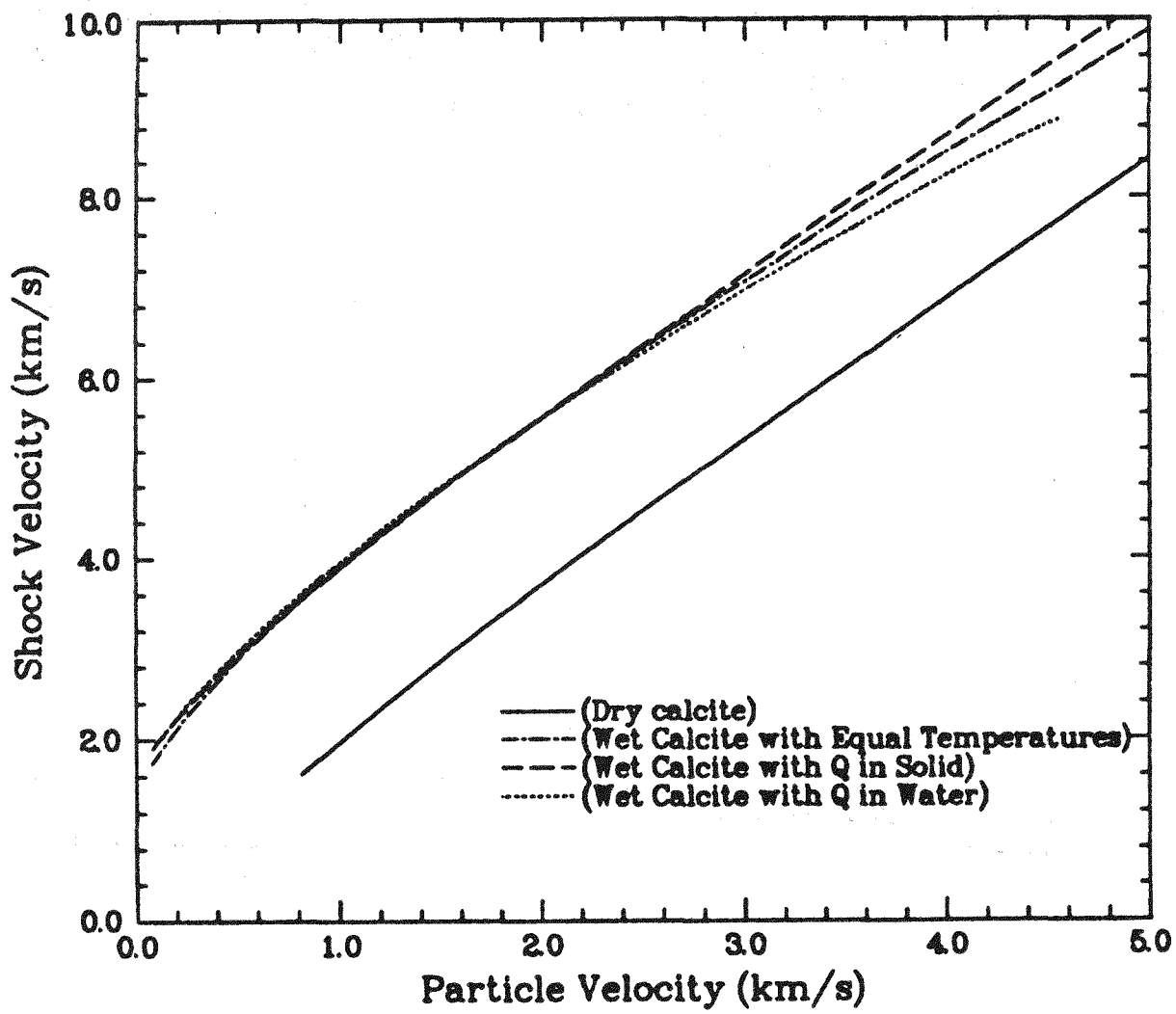

Figure 30: Computed Hugoniot States for the Wet and Dry Samples used in this Work.

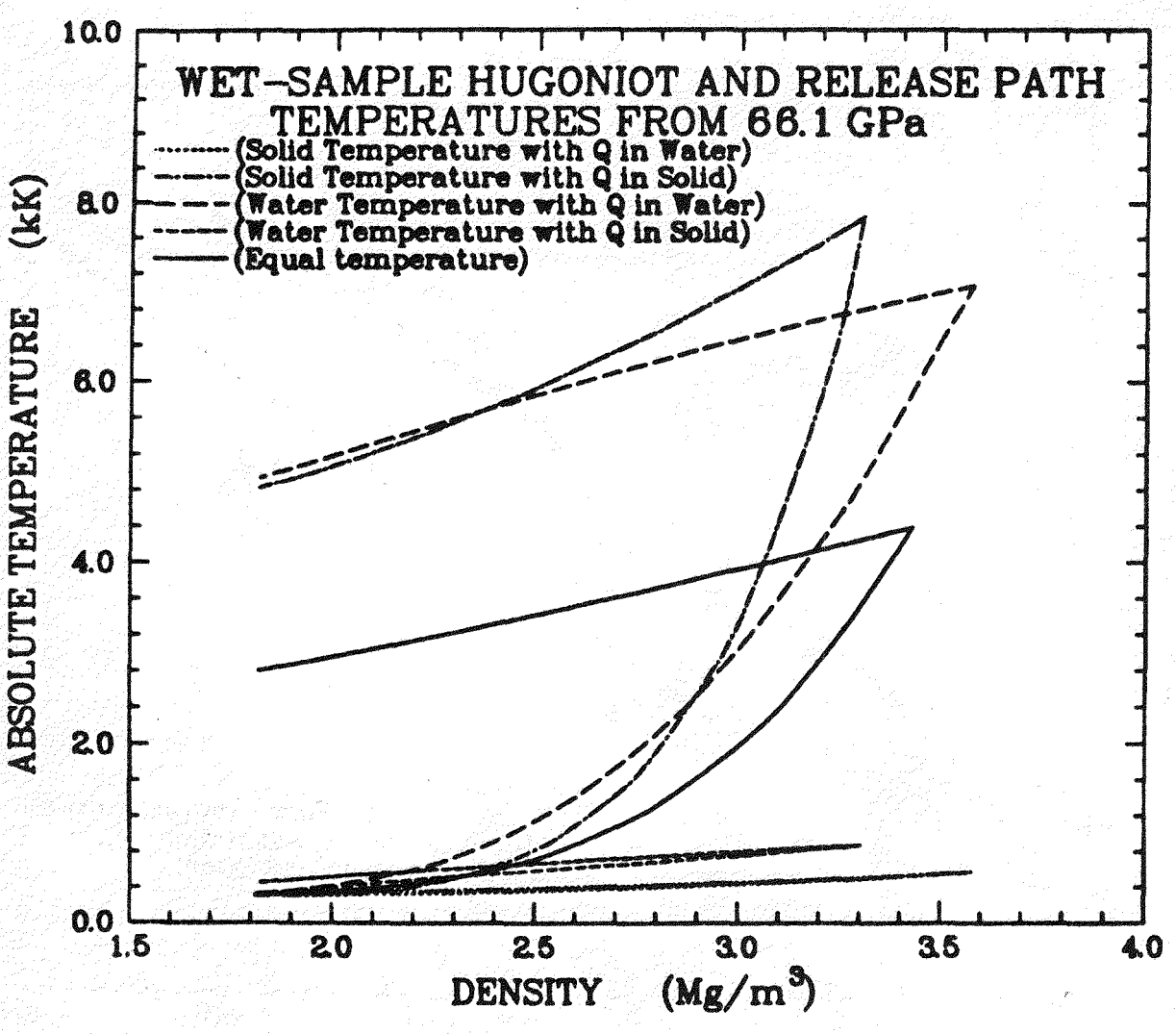

Figure 31: Computed Temperatures for the Wet and Dry Samples used in this Work.

(Kipp and Lawrence, 1981). The version of the model used in this code includes the effects of intergranular contact. The selected values for the parameters in Equation 5.13 are $\tilde{\phi}_{sm} - \phi_{s0} = 0.1$, $\bar{\rho}_{s0}\Omega_m = 4$ GPa, and $n = 2.5$. The additional parameter required by Equation 5.15 is $\rho_{s0}\Omega_e = 0.1$ GPa. Thus in the dry porous samples, crushing of the granules is assumed to begin at a pressure of 0.1 GPa. Completion of crushing is at 4 GPa. Also, upon release from pressures above 4 GPa, 10-percent porosity is recovered in the sample. When compared against the Hugoniot and release-path calculations in the previous section, this version of the model did not produce appreciably different results from the equal-pressure version in which no porosity is recovered.

Figures 33 thru 35 contain the comparisons of the calculations to the data obtained from experiments CA-16, 17, and 18 on the dry calcite powder. Figures 36 thru 38 contain the comparisons to CA-19, 20, and 21 on the wet samples. Because of timing problems in these experiments, the experimental data were arbitrarily time-shifted into alignment with the computed wave profiles. Two shock waves appear in each comparison since the gap between the flyer plate and its holding fixture closed during the time data were collected. The aluminum components of the experimental configuration were modeled as elastic-plastic, with an instantaneous spall threshold of 1 GPa. The calculations indicate that extensive spallation occurred on the back of the flyer plate. This was subsequently recompacted by the holding fixture. This is the source of noise in the computed profile of the second wave.

In general, the comparisons for the first stress wave are quite good. The time spacing between the first and second wave are better for the wet samples than for the dry samples. Here, the spacing for the dry samples is a little too rapid. The comparison of the profiles for the second waves is poor. The reason for these discrepancies is not known.

In addition to the comparisons for the measured particle-velocity profiles discussed above, comparisons of the pressure-density release trajectories at the data plane are given in Figures 39 and 40. The calculations show good agreement with the experimental results from the dry samples. The comparisons with the wet samples are poor. The experimental results were reduced using the measured wave velocities. Thus the effect of time shifting, which was used in the comparisons of the wave profiles, is not present in the data reduction.

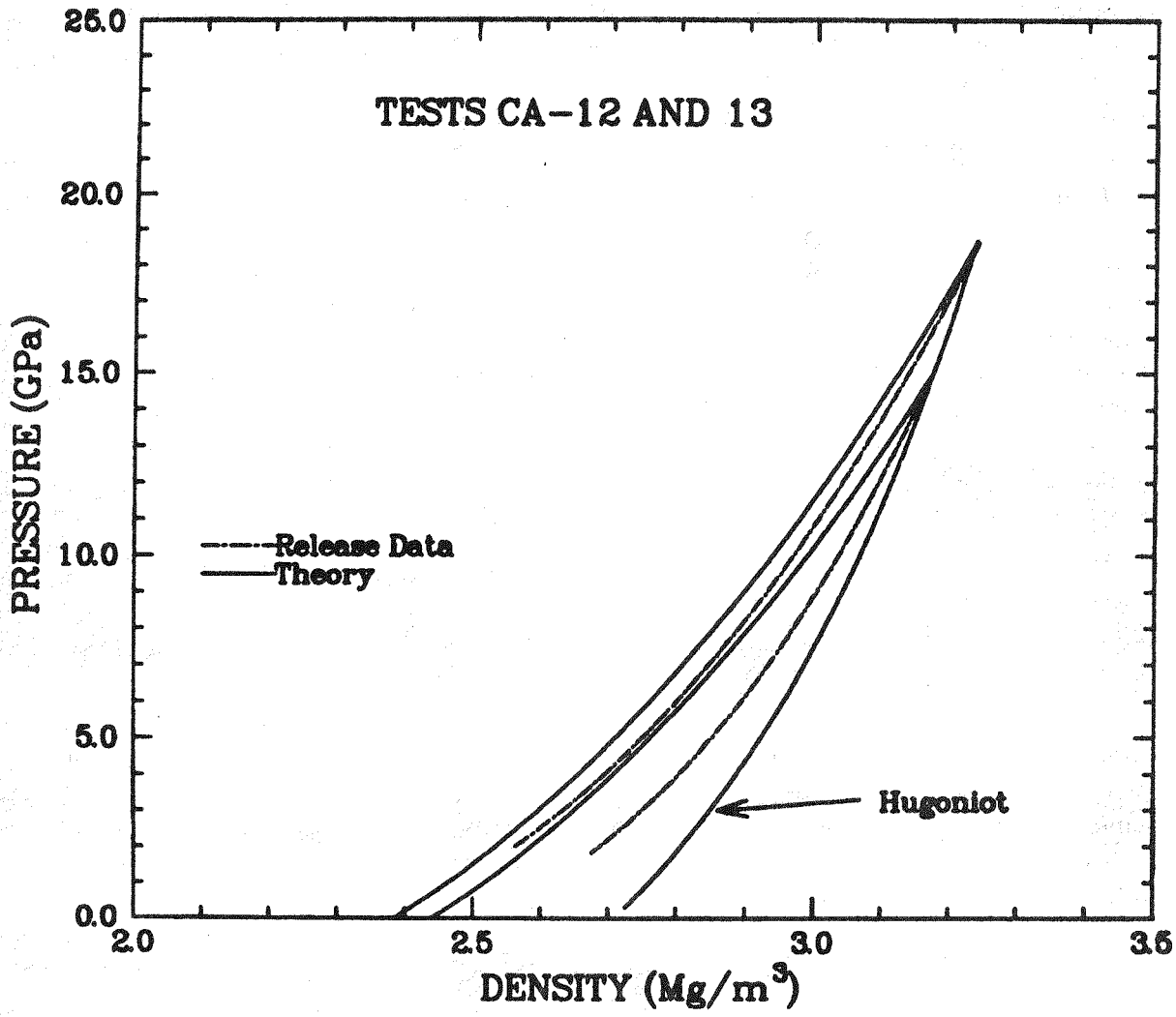

Figure 32: Computed Hugoniot and Release Paths for CA-12 and CA-13.

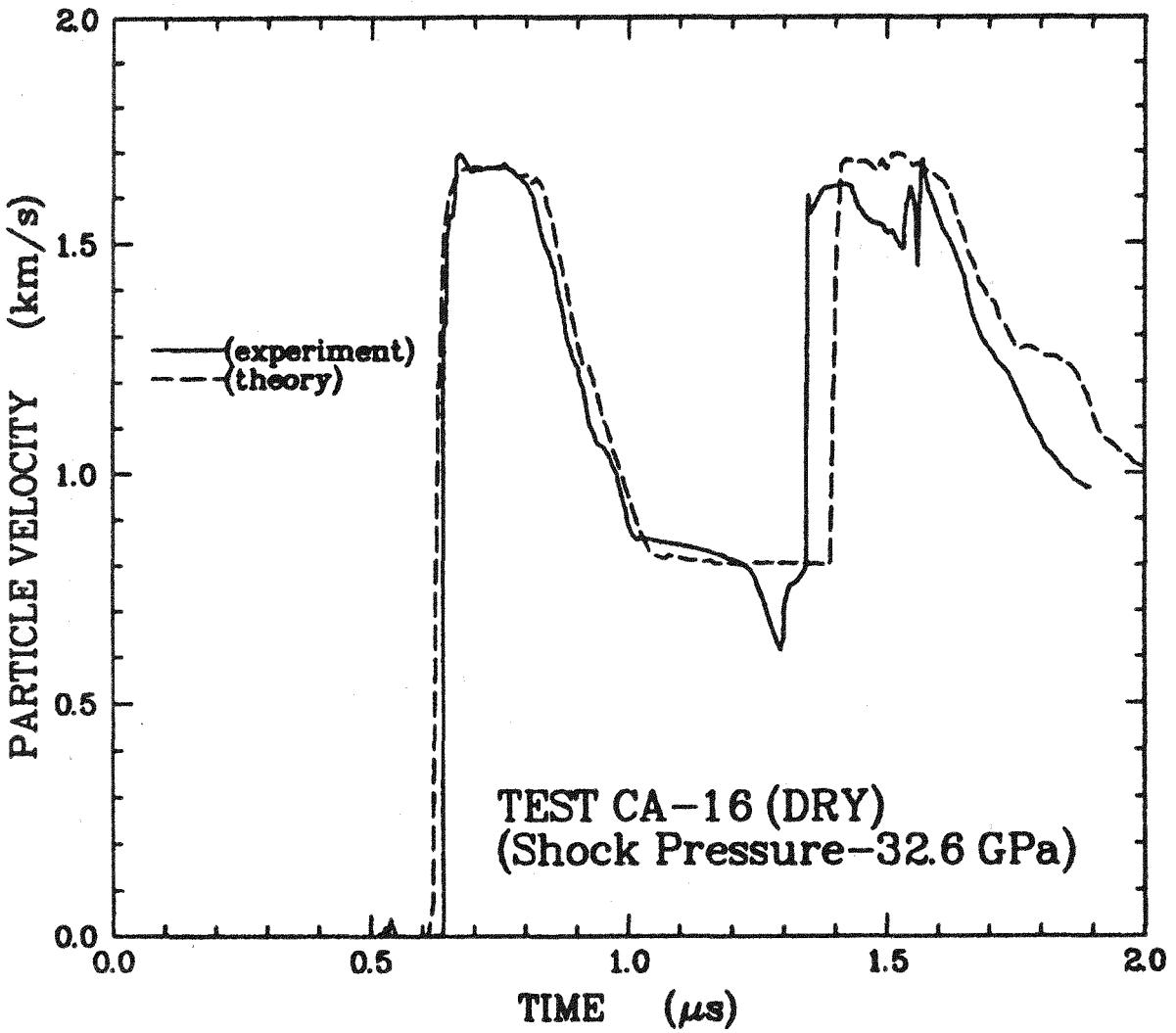

Figure 33: Comparison of Theoretical Prediction to CA-16.

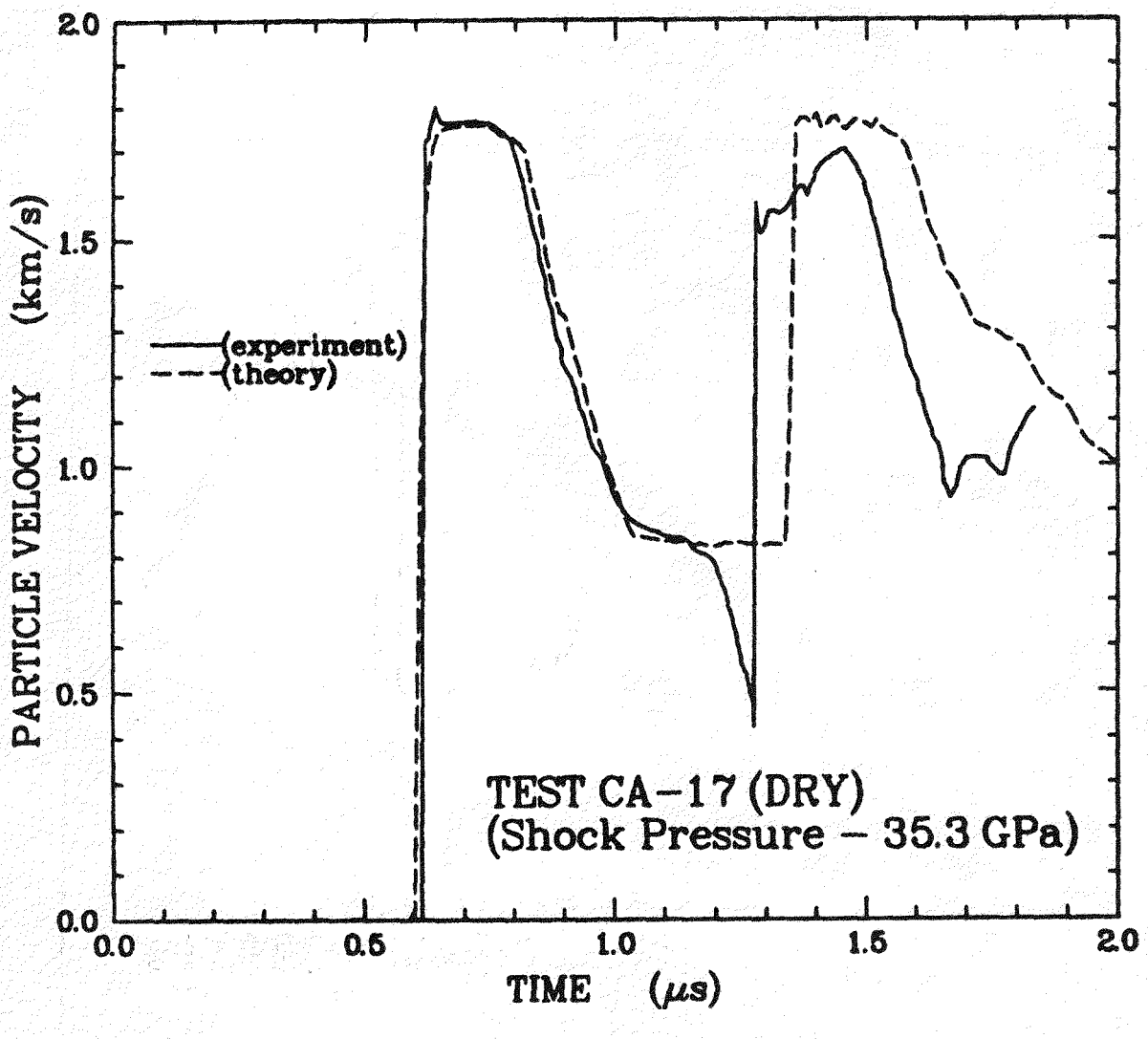

Figure 34: Comparison of Theoretical Prediction to CA-17.

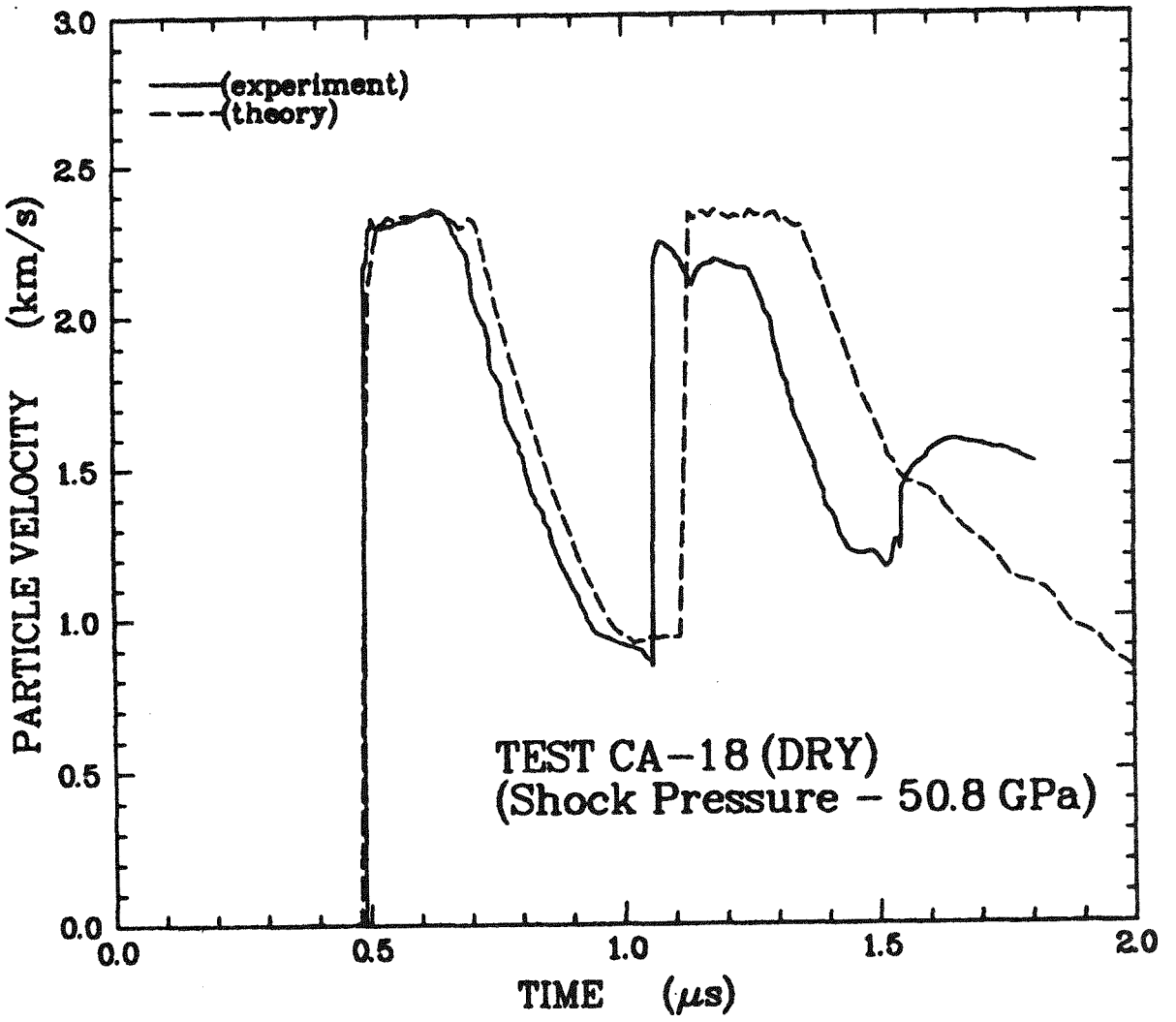

Figure 35: Comparison of Theoretical Prediction to CA-18.

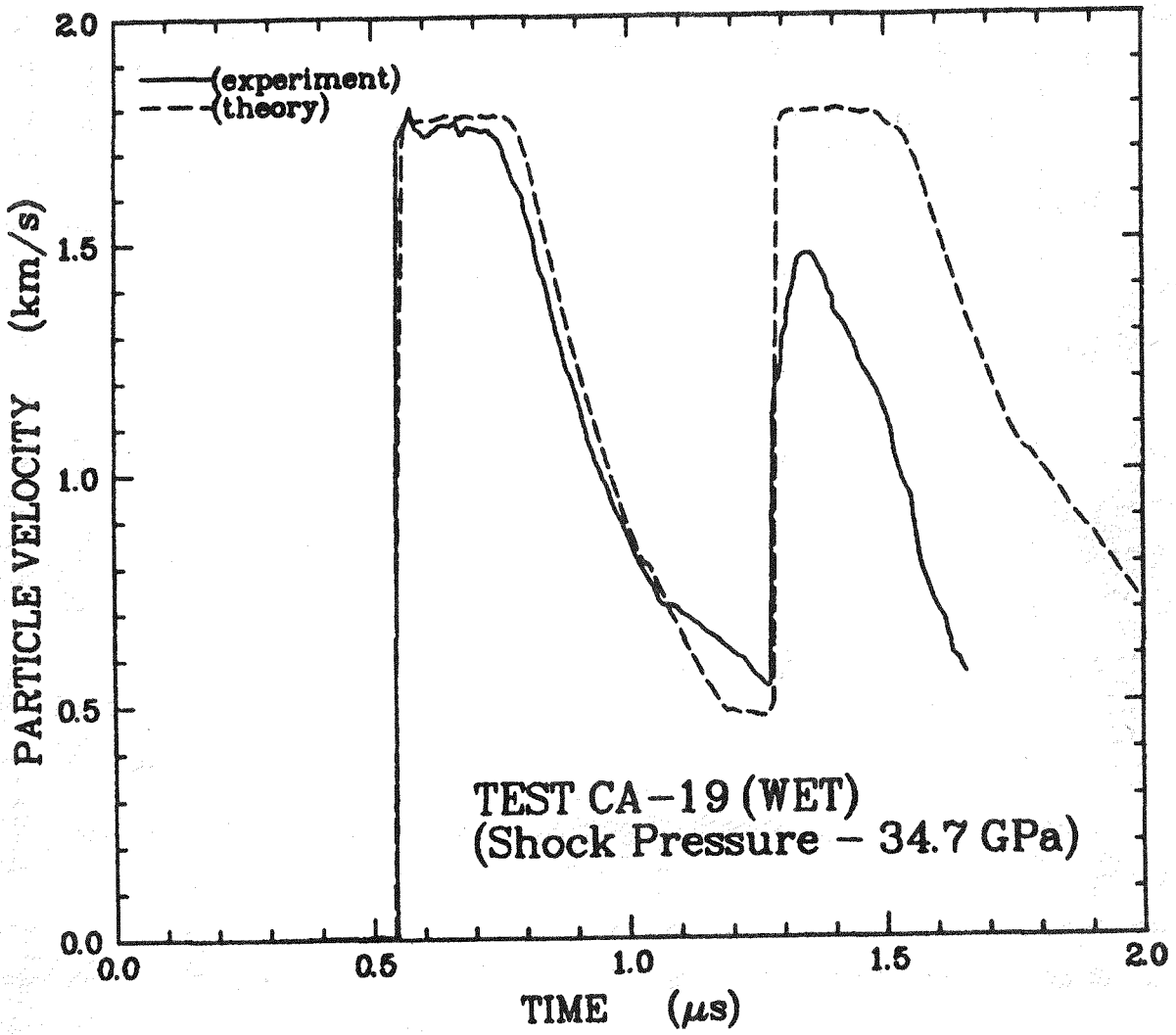

Figure 36: Comparison of Theoretical Prediction to CA-19.

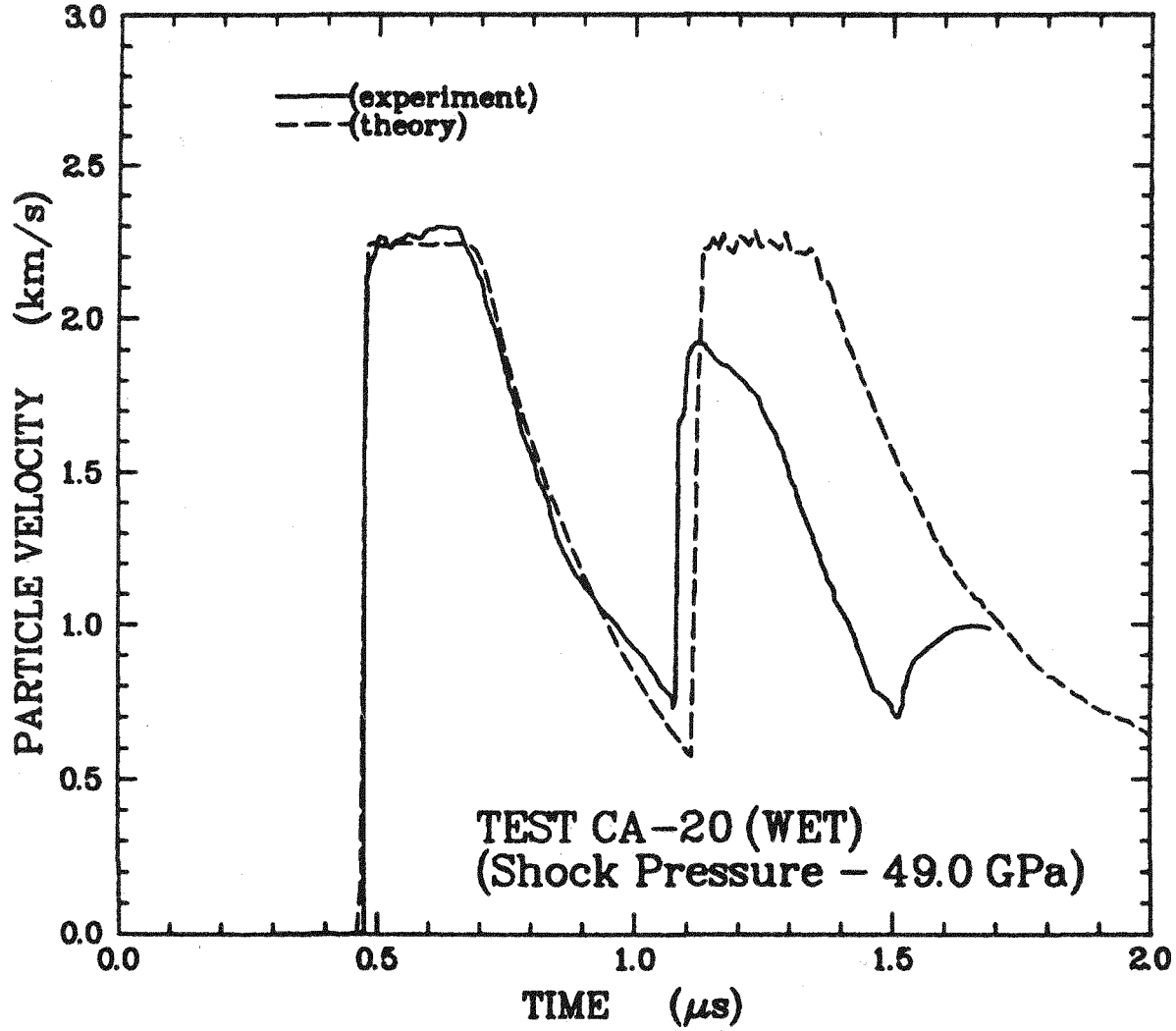

Figure 37: Comparison of Theoretical Prediction to CA-20.

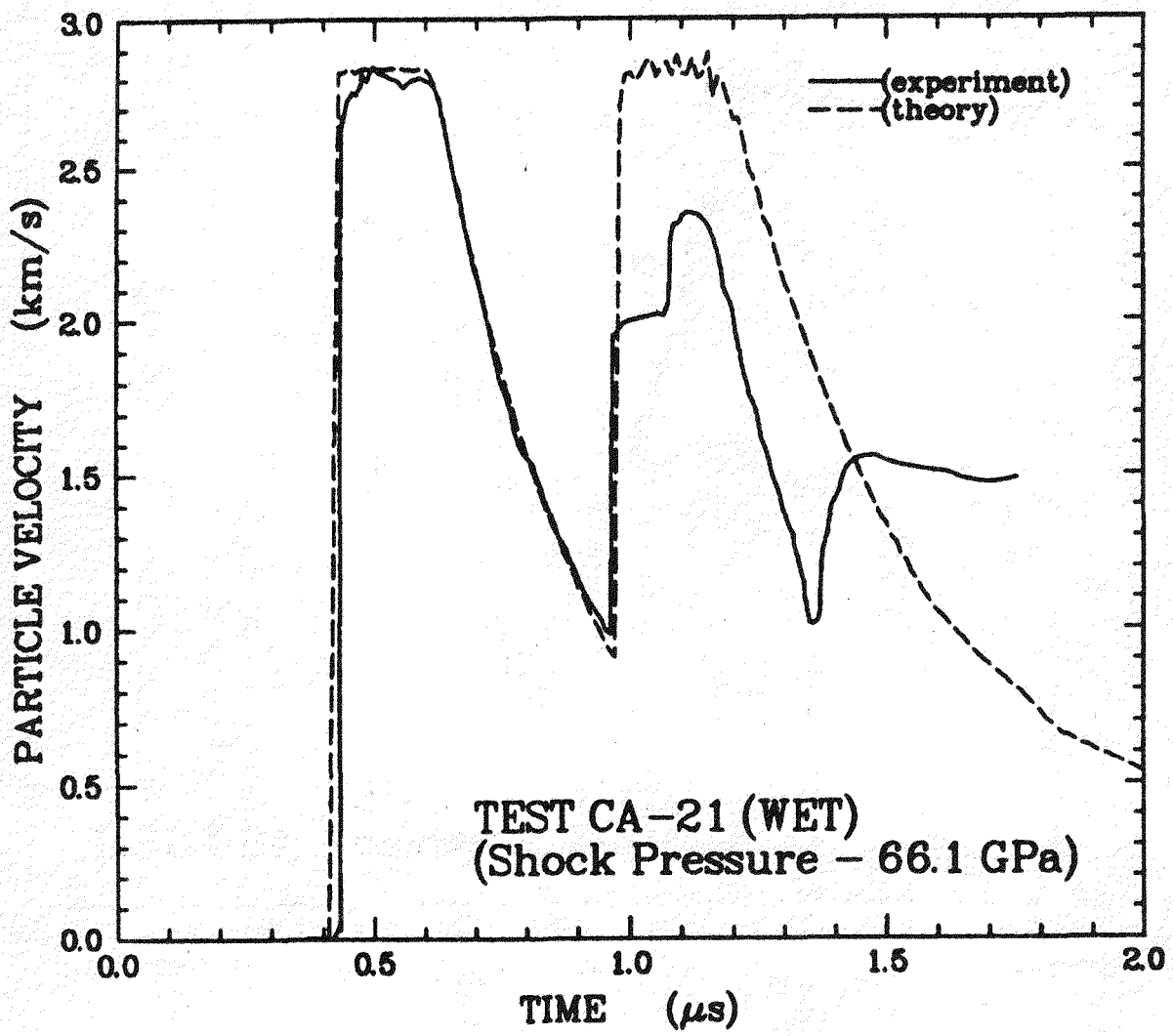

Figure 38: Comparison of Theoretical Prediction to CA-21.

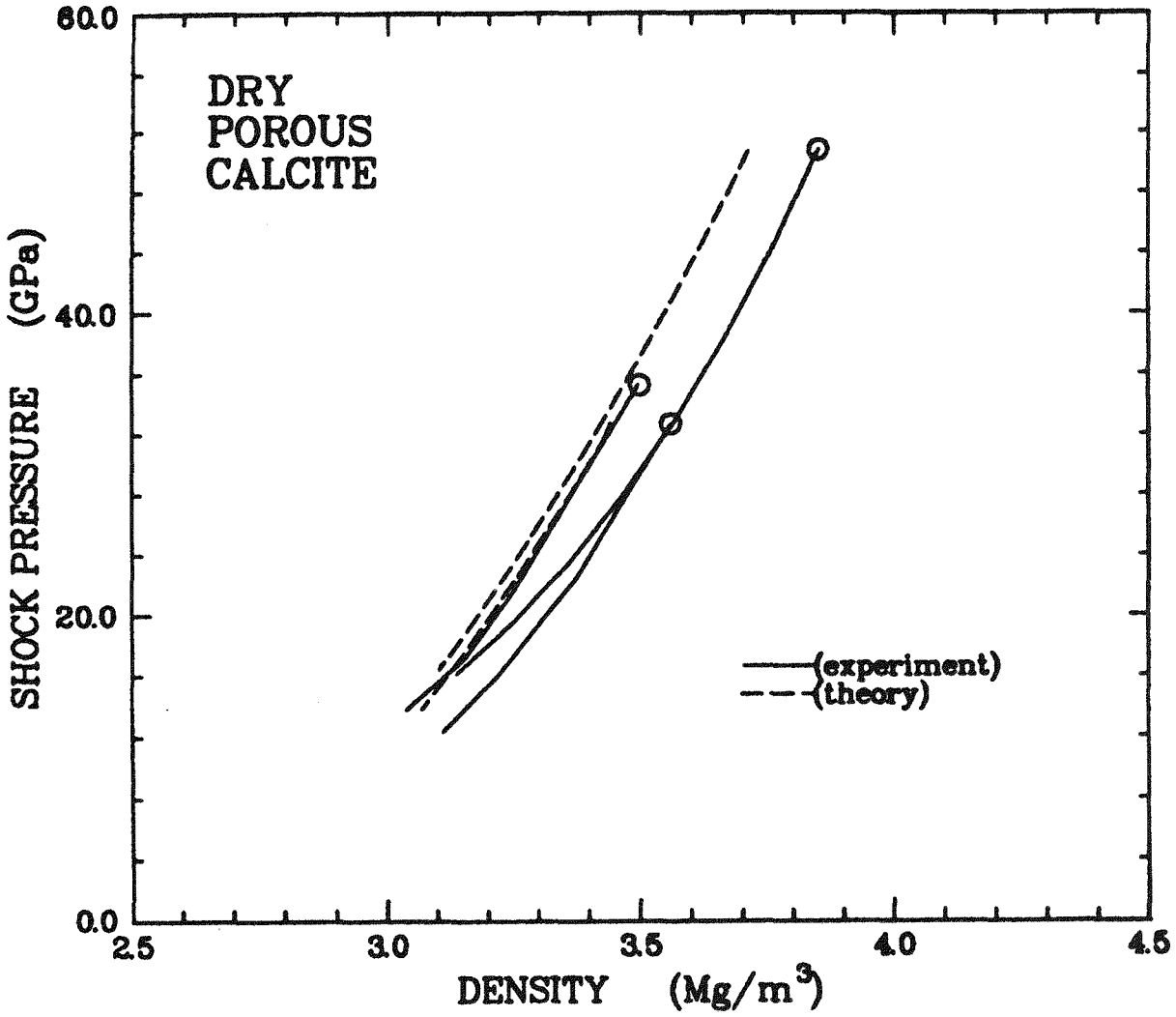

Figure 39: Comparison of Theoretical Release Paths to Data from Dry Samples.

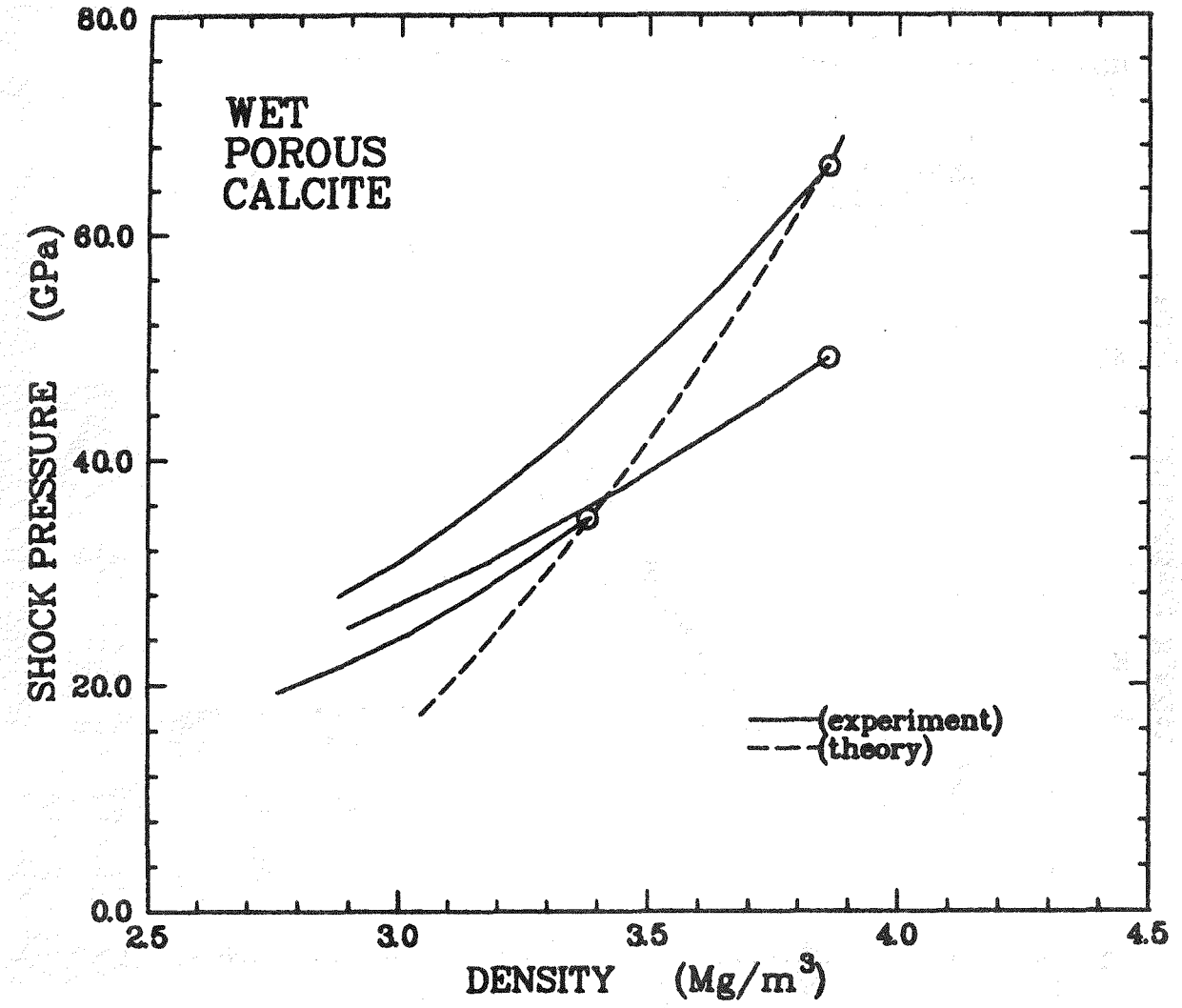

Figure 40: Comparison of Theoretical Release Paths to Data from Wet Samples.

6 CONCLUSIONS AND RECOMMENDATIONS FOR FURTHER STUDY

During the present program, considerable progress in the development of technology for measuring high-pressure shock and release equation-of-state data on dry- and water-saturated porous geological materials was achieved. Useful data on crystalline, dry-porous, and water-saturated calcite was obtained. A model based on a theory of immiscible mixture was developed and successfully applied.

Some new physics was revealed in the experimental data. Although earlier data hinted at a phase transformation in calcite in the range of about 9 to 16 GPa, the present study clearly identified this transition between 12–14 GPa through a striking rarefaction shock wave. This in-of-itself is quite unique—attesting to the rapid transformation rate and near equilibrium behavior of this transition under shock compression and release. In contrast, similar shock-induced transitions in silicate minerals show rate sensitivity through dispersive release waves and metastable Hugoniot states.

Experiments on porous calcite in the present study did not, however, reveal evidence for this transition. Reasons for this are not known. A possible explanation is a reduction of the transformation volume with temperature depressing the range of anomalous compressibility. This problem deserves further study, working with a range of porosities to better map out the temperature dependence.

No clear indication of melting is provided by the wave-profile data, although the requirement of a decreasing Grüeissen parameter in the theoretical model to reproduce the experimental data lends support for theories which predict a decrease of this parameter with temperature in the liquid state. This further suggests that the calcite is probably deep into the liquid state after shock compression from the initial dry porous state.

Although the degree of thermal heterogeneity persisting at the shock state and during release is not known, bounding calculations based on the present immiscible mixture model for calcite indicates that stress-wave propagation properties are not strongly sensitive to this issue.

As the present experimental program evolved, several experimental difficulties were uncovered. Foremost was an inconsistency in measured sample transit times and, therefore, shock velocities. Several possible explanations exist. First, sample thicknesses are necessarily small leading to general random errors in measuring transit times. This, however, is not sufficient to explain the magnitude of the discrepancy. The pins used to measure time-of-impact are an electrical shorting type where shock impact closes an approximately 50-μm gap between copper electrodes. Although transit for this gap is accounted for at these impact pressures, possible jetting and premature shorting render this transit time ambiguous. Improved techniques are needed here.

A further possible problem occurs if the cavity projectile allows settling of the impact plates during acceleration. This would lead to measured transit times larger than actual.

In general, measure shock velocities are less than measured by Kalashnikov, *et al.* (1973) and predicted by the model based principally on Kalashnikov, *et al.* (1978) data. The discrepancy is larger for wet than for dry samples. This trend is not understood but might explain differences between data and calculation for the water-saturated release curves in Figure 40.

Another possible source of error would occur if full water saturation were not achieved in the porous samples. An independent measure of the water content was not made and it is not known if an inaccessible void fraction exists. This could lead to further errors in analysis and calculation of the water-saturated data.

Thus, there is a need for a further look at these experimental difficulties and a broader data base on the shock and release properties of porous materials subject to varying degrees of water content. Despite some problems, however, significant strides in technique development have been made during this study and the release data when combined with earlier Hugoniot data on calcite provide a valuable constraint on computational models as attested to by the theoretical study in the present work.

7 REFERENCES

Adadurov, G. A., D. B. Balshov, and A. N. Dremin, "A Study of the Volumetric Compressibility of Marble at High Pressure," *Isv. Acad. Sci. USSR Phys. Solid Earth*, Eng. Trans. No. 5, 463-466 (1961).

Ahrens, T. J. and V. G. Gregson, "Shock Compression of Crustal Rocks: Data for Quartz, Calcite, and Plagioclase Rocks," *J. Geophys. Res.*, **69**, 4839-4874 (1964).

Al'tshuler, L. V., K. K. Krupniskev, B. N. Ledenev, V. T. Zhnchikhin, and M. I. Brahgnik, Dynamic Compressibility and Equation of State of Iron Under High Pressure, Sov. Phys. JETP, **34**. 606 (1958).

Asay, J. R., private communication.

Barker, L. M. and R. E. Hollenbach, "Laser Interferometry for Measuring High Velocity of any Reflecting Surface," *J. Appl. Phys.*, **43**, 4669 (1972).

Chhabildas, L. C. and J. R. Asay, "Risetime Measurements of Shock Transitions in Aluminum Copper, and Steel," J. Appl. Phys., **50**, 27-49 (1979).

Dmitriyev, A. P., *et al.*, NASA Technical Translation, NASA TT F-684, June 1972.

Drumheller, D. S. and A. Bedford, Arch. Rat. Mech. Anal., "A Thermomechanical Theory for Reacting Immiscible Mixtures," **73**, 257-284 (1980).

Drumheller, D. S., "A Theory for Dynamic Compaction of Wet Porous Solids," *Int. J. Solids Struct.*, in press.

Grady, D. E., "Stress-Wave Experiments on Selected Crustal Rocks and Minerals," Sandia National Laboratories Report, SAND83-1898, September 1983.

Grady, D. E. and E. G. Young, "Evaluation of Constitutive Properties from Velocity Interferometer Data," Sandia National Laboratories Report, SAND75-0650, August 1976.

Herrmann, W., "Constitutive Equation for the Dynamic Compaction of Ductile Porous Materials," *J. Appl. Phys.*, **40**, 2490-2499 (1968).

Kalashnikov, N. G., M. N. Pvlovskiy, G. V. Simakov, and R. F. Trunin, "Dynamic Compressibility of Calcite-Group Minerals," *Izv., Earth Physics*, **2**, 23 (1973).

Kerley, G. I., "Theoretical Equations of State for the Detonation Products of Explosives," Proc. Eighth Sym. on Detonation, July 15-19, 1985.

Kipp, M. E. and R. J. Lawrence, "WONDY V-A One-Dimensional Finite-Difference Wave Propagation Code," Sandia National Laboratories Report SAND81-0930, 1981.

Konrad, C. H. and R. L. Moody, "Rear Surface Pin Triggering Technique," Sandia National Laboratories Report SAND86-0791 (1986).

Tyburczy, J. A. and T. J. Ahrens, "Dynamic Compression and Volatile Release from Carbonates," *J. Geophys. Res.*, to be published.

Visgirda, J. and T. J. Ahrens, "Shock Compression of Aragonite and Implications for the Equation of State of Carbonates," *J. Geophys. Res.*, **87**, 4747-4758 (1982).

Wise, J. L. and L. C. Chhabildas, "Laser Interferometer Measurements of Refractive Index in Shock Compressed Materials," Proceedings of the Topical Conference on Shock Waves, July 22–26, 1985, Spokane, Washington (to be published).

Distribution:
Don Simmons
R&D Associates
Post Office Box 9695
Marina del Rey, CA 90291

Steve Melzer
Science Applications, Inc.
Post Office Box 2083
Midland, TX 79702

B. Dibona
Terra Tek
420 Wakara Way
Salt Lake City, UT 84108

Ed Tremba
System Science and Software
Post Office Box 8243
Albuquerque, NM 87198

Shel Shuster
California Research and Technology
20945 Devonshire
Charsworth, CA 91311

Stephen Peyton
System Science and Software
Post Office Box 8243
Albuquerque, NM 87198

Don Burton
Lawrence Livermore National Laboratory
Post Office Box 808, L-200
Livermore, CA 94550

Tom Ahrens
California Institute of Technology
MS/252-21
Pasadena, CA 91125

Sandia Internal:
1510 J. W. Nunziato
1520 D. J. McCloskey
1530 L. W. Davison
1531 S. L. Thompson
1531 J. W. Swegle
1533 P. Yarrington
1534 J. R. Asay
1534 L. C. Chhabildas
1534 D. E. Grady (15)
1534 R. L. Moody (15)
1540 W. C. Luth
1550 R. C. Maydew
3141 S. A. Landenberger (5)
3151 W. L. Garner (3)
3154-4 C. H. Dalin (28)
For DOE/OSTI
6242 D. S. Drumheller (15)
8024 P. W. Dean